Earth-Science Reviews 262 (2025) 105061

Contents lists available at ScienceDirect

Earth-Science Reviews

journal homepage: www.elsevier.com/locate/earscirev

Review Article

Influences of paleoclimatic changes on organic matter enrichment mechanisms in freshwater and saline lacustrine oil shales in China: A machine learning approach

Man Lu [a,b,c], Guoqiang Duan [a,b,c], Tongxi Zhang [a,b,c], Naihao Liu [d], Yuxuan Song [a,b,c], Zezhou Zhang [d], Jinqi Qiao [a,b,c], Zhaoyang Wang [a,b,c], Zilong Fang [a,b,c], Qingyong Luo [a,b,c,*]

[a] Hainan Institute of China University of Petroleum (Beijing), Sanya 572025, China
[b] State Key Laboratory of Petroleum Resources and Engineering, China University of Petroleum (Beijing), Beijing 102249, China
[c] College of Geoscience, China University of Petroleum (Beijing), Beijing 102249, China
[d] School of Information and Communications Engineering, Xi'an Jiaotong University, Xi'an 710049, China

ARTICLE INFO

Keywords:
Lacustrine oil shales
Organic matter
Paleoclimate
Machine learning
Geochemical characteristics
Depositional environments

ABSTRACT

Lacustrine oil shales are valuable unconventional resources, with their organic matter (OM) enrichment closely linked to paleoclimatic conditions. However, the mechanisms controlling OM enrichment in freshwater and saline lacustrine environments remain underexplored. This study represents the first application of the random forest (RF) classifier to investigate how paleoclimatic changes influence OM enrichment mechanisms in lacustrine oil shales in China. By analyzing the bulk geochemical (total organic carbon (TOC), trace and major elements) and molecular biomarker data from seven representative lacustrine oil shales, we demonstrate that the RF classifier can effectively discriminate between freshwater and saline lacustrine oil shales. The results indicate that the TOC content is the most significant parameter, with freshwater shales having higher TOC values than their saline counterparts. Further analyses suggest that OM enrichment in these two types of lacustrine settings was driven by a combination of factors, including paleoproductivity, paleowater conditions, and terrigenous inputs, all modulated by paleoclimatic changes. Freshwater lacustrine shales were generally deposited during humid and warm periods with higher atmospheric CO_2 levels and greater precipitation, which led to higher paleoproductivity, reduced terrigenous influx, rising lake levels, and improved OM production and preservation. In contrast, saline lacustrine shales were deposited during dry and cold periods, when increased water salinity and diminished paleoproductivity resulted in lower OM production, reduced preservation, and decreased TOC content. These findings provide key insights into the role of paleoclimate in shaping OM-rich lacustrine shales and establish a framework for evaluating organic-rich shale deposits. The study also underscores the potential for future geochemical datasets to enhance classification models and broaden applications of machine learning in the exploration of hydrocarbon resources.

1. Introduction

As conventional oil and gas resources become increasing depleted, unconventional resources, such as shale oil and shale gas, have thus become critical replacements, especially in fast-growing markets such as China. Oil shale resources in China are estimated at 987 billion tons, equivalent to 61 billion tons of in-place shale oil, with most found in lacustrine oil shale sequences (Liu et al., 2009; Ministry of Land and Resources of China, 2006). Since organic matter (OM) is the foundation for forming source rocks, understanding the mechanisms behind OM enrichment in lacustrine oil shales is essential for optimizing unconventional resource exploration and contributing to energy security and sustainability. Furthermore, lacustrine basins, being relatively restricted systems, are particularly sensitive to climate perturbations, making OM enrichment closely linked to variations in sedimentary environments (Castañeda and Schouten, 2011). Therefore, the study of OM enrichment processes in lacustrine shales provides valuable insights into past environmental changes and serves as a record of continental paleoclimate and paleoenvironment shifts (Anderson and Dean, 1988; Chamberlain et al., 2013; Wang et al., 2017).

* Corresponding author at: Hainan Institute of China University of Petroleum (Beijing), Sanya 572025, China.
E-mail address: qingyong.luo@cup.edu.cn (Q. Luo).

https://doi.org/10.1016/j.earscirev.2025.105061
Received 4 November 2024; Received in revised form 11 January 2025; Accepted 2 February 2025
Available online 7 February 2025

In China, shale oil exploration has mainly focused on shales in saline lacustrine basins, including the early-middle Permian Fengcheng and Lucaogou formations in the Junggar Basin, and the Eocene Shahejie and Kongdian formations in the Bohai Bay Basin. Recent significant advancements have been made in exploring the freshwater lacustrine basins in China, such as the Upper Triassic Yanchang Formation in the Ordos Basin and the Upper Cretaceous Qingshankou Formation in the Songliao Basin. These advancements highlight the critical role both freshwater and saline lacustrine basins play in oil shale formation. Freshwater and saline lacustrine systems differ fundamentally in their hydrological and chemical conditions, which in turn influence the OM production, preservation, and enrichment in sediments. In the modern world, freshwater lakes, typically dominated by river inflow and precipitation, generally support higher biological productivity, promoting OM accumulation. In contrast, saline lakes are often characterized by restricted inflow and high evaporation rates, leading to elevated salinity levels. These conditions may result in lower organic productivity but higher preservation of specific organic compounds, which influences quality and quantities of OM accumulated in the sediments. Climate factors, such as temperature, precipitation, and evaporation rates, exert profound influences on these processes, complicating the mechanisms of OM enrichment across these contrasting environments. However, the relationship between OM enrichments in the freshwater and saline lacustrine shales and paleoclimate variations over geological time has not been fully established.

Previous studies have investigated OM enrichment mechanisms in Chinese lacustrine oil shales in the context of paleoclimate changes. However, many of these studies either focused on the geochemical characteristics of an individual oil shale formation in a single region (e.g., Ma et al., 2016; Chen et al., 2019; Li et al., 2024c) or present an overview of a single type of lacustrine oil shale (Jin and Zhu, 2006; Xu et al., 2024), while others focused on comparing marine OM-rich shales with lacustrine ones (Warren, 2010; Zou et al., 2019). To our knowledge, no previous studies have systematically analyzed the differences in geochemical characteristics and OM enrichment mechanisms between freshwater and saline lacustrine oil shales. One key challenge lies in the complex, nonlinear interactions between climatic variables and geochemical processes that govern the OM enrichment, making it difficult to draw definitive conclusions about the climatic mechanisms influencing OM enrichment in different lacustrine setting.

To address these challenges, this study applied random forest (RF) algorithm, a machine learning technique, to analyze the multivariate relationships involved in OM enrichment. The RF classifier is one of the most widely used algorithms for classification problems (Singh et al., 2016). It consists of a group of decision trees, where each tree can make the classification decision by asking a sequence of true-or-false questions. RF is particularly effective at minimizing human bias and facilitating more reliable conclusions. Thanks to its learning capability, RF is well-suited to handling large and complex datasets (Reichstein et al., 2019; Herzsprung et al., 2020), making it ideal for identifying differential patterns of OM enrichment in both freshwater and saline lacustrine environments and understanding the regulatory factors involved. Unlike traditional statistical methods, RF can capture complex relationships and interactions between variables, including nonlinear, non-monotonic and multidimensional linear responses of data structure, providing deeper insights into the processes involved. Recent studies have successfully used RF in geoscience fields, such as atmospheric biogeochemistry (Osterholz et al., 2016; Shi et al., 2022), remote sensing of land surfaces (Lary et al., 2016; Pan et al., 2020), ore deposits (Hoggard et al., 2020; Zhou et al., 2023) and chemometric trends in the modern and ancient oceans (Mahynski et al., 2022; Wang et al., 2023c). However, the application of big data and machine learning methods is still in its infancy in oil shale research.

In this study, we compiled the geochemical characteristics of freshwater and saline lacustrine oil shales and employed the RF to investigate the climate-driven differential OM enrichment mechanisms in major lacustrine oil shales in China (Fig. 1). Through analyzing comprehensive datasets from both freshwater and saline lacustrine oil shales, we infer the paleoclimatic conditions in these lacustrine basins and their influence on depositional environments and processes. We then explored the relationship between OM enrichment and paleoclimate across these lacustrine settings, ultimately seeking to uncover the specific paleoclimatic conditions that favored OM accumulation and preservation in each environment. The findings of this research have important implications for enhancing our understanding of lacustrine oil shale formation and advancing exploration strategies in lacustrine basins, both in China and globally.

2. Methods

2.1. Data synthesis

This study is based on a comprehensive review of the published literature on the geochemical characteristics of lacustrine oil shales in China. Although lacustrine organic-rich shale units are widely recognized in Mesoproterozoic through Cenozoic strata (Jin et al., 2023) and are extensively distributed across China (Zou et al., 2019), this analysis focuses on data synthesis from only seven lacustrine oil shales: the seventh member of the Yanchang Formation (Chang 7) in the Ordos Basin, the Qingshankou Formation in the Songliao Basin, the Fengcheng and Lucaogou formations in the Junggar Basin, and the Shahejie and Kongdian formations in the Bohai Bay Basin (Fig. 1) (see Geological Setting in Supplementary Material). Prior to the machine learning analyses, the selected oil shales were classified into freshwater and saline lacustrine oil shales. It is important to note that the salinity of these basins was not constant over time. For example, during the deposition of the Qingshankou Formation, episodic marine incursions probably contributed to periods of increased salinity within the lacustrine basins. The classification scheme adopted in this study follows Li et al. (2022a), which is based on overall sedimentary patterns of the oil shales. Specifically, the Chang 7 and Qingshankou formations are classified as freshwater lacustrine shales, whereas the remaining five formations are classified as saline lacustrine shales (Li et al., 2022a). These basins are recognized for their commercial potential, housing oil shales deemed significant hydrocarbon source rocks and targets for shale oil exploration (Jia et al., 2012). The selection of these oil shales was guided by two main criteria: i) they represent major hydrocarbon source rocks and targets for shale oils in the basins where they are distributed; and ii) the availability of previously published raw data on their inorganic and organic geochemical characteristics. Due to the absence of a publicly available database for China's oil shale records in existing literature or online platforms, we compiled our dataset exclusively from peer-reviewed journal publications. For studies that did not provide raw data directly, the data from the graph were digitized using GETDATA software (GetData Graph Digitizer version 2.20). Unpublished sources, such as personal webpages and private materials, were completely excluded. To perform the literature search, the formation names were used as keywords in Google Scholar and the Web of Science. Original research articles were further verified through a cross-reference in original journal websites and major databases, such as ScienceDirect and China National Knowledge Infrastructure. The literature search was conducted from August 2023 to January 2024, and studies published after the January 2024 were not included in our dataset.

Our initial compiled dataset included 147 proxies, encompassing absolute concentrations of trace metals, major oxides, and molecular biomarker compounds. Given that these absolute concentrations were obtained using various analytical methods, instrumental techniques and quality-control protocols, which can introduce uncertainties, we normalized concentrations and utilized ratios between different trace metals, major oxides and biomarker compounds. Prior to the RF analysis, we converted the ratios between some oxides to the corresponding elemental ratios. For example, we transformed the P_2O_5/Al_2O_3 ratio into

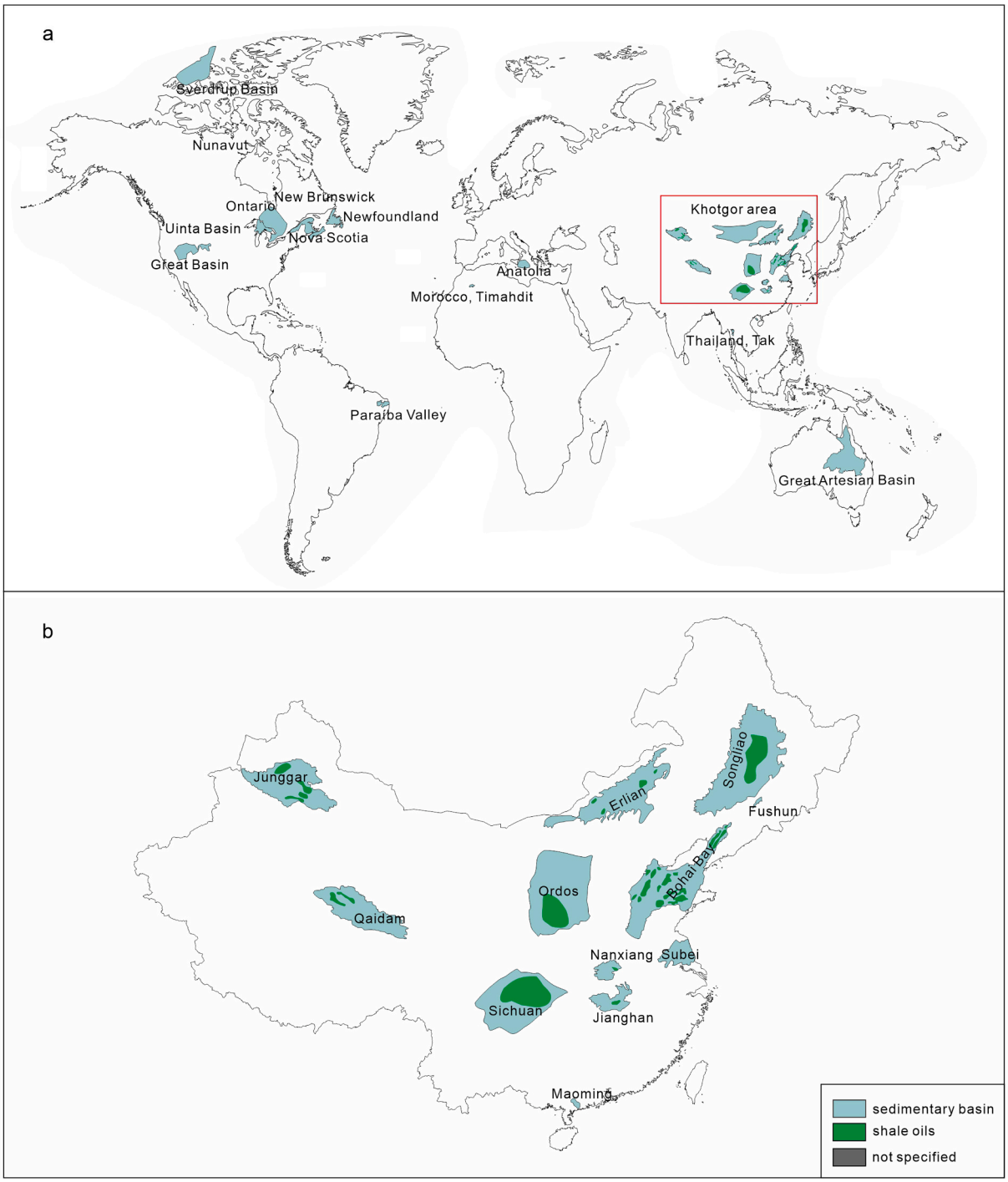

Fig. 1. Simplified map illustrating a) the global distribution of lacustrine oil shales, labeled according to their respective depositional basins, and b) the distribution of major lacustrine shale oils in China. The red rectangle in panel (a) highlights the major lacustrine oil shales in China. Detailed information on the oil shales and their corresponding depositional basins are provided in Table 1. (For interpretation of the references to colour in this figure legend, the reader is referred to the web version of this article.)

the P/Al ratio by utilizing the stoichiometric relationship between the elements and their oxides. As for redox-sensitive trace metals, Al-normalized enrichment factors (EFs) were calculated relative to the post-Archean Australian Shale (PAAS) ($EF = [metal/Al]_{sample}/[metal/Al]_{PAAS}$), where PAAS values for Al and individual trace metals were from Taylor and McLennan (1985). Proxies associated with thermal maturity and degradation, such as the Rock-Eval T_{max} parameter, C_{29} steranes 20S/(20S + 20R), and sterane ββ/(αα + ββ), were excluded from analysis. Proxies with incomplete data across two types of oil shales were also omitted. Additionally, outlier samples with proxy values exceeding three standard deviations from the mean were removed from machine learning analyses, resulting in a 1.25 % deletion rate. After the screening process, we retained 15,444 entries from 32 proxies and 3841 samples (Supplementary Dataset 1).

2.2. Statistical methods

The random forest (RF) classifier was built in *scikit-learn* Python 23.2

software (Python Software Foundation, Wilmington, DE, USA). Before training the classifier, all variables were standardized using the formula: $y' = (y - \mu)/\sigma$, where y' is the standardized value, y is the original value, μ and σ are the average and standard deviation of the dataset of y, respectively. During RF analysis, the lacustrine oil shale dataset was randomly divided into two subsets by a bootstrap method: the large subset for training and a smaller subset for testing the accuracy of oil shale type assignments (i.e., distinguishing between freshwater versus saline lacustrine oil shales). Samples of each setting were randomly split into these two subsets in a ratio of 4:1. The k-fold cross-validation was also employed to enhance the performance of our model on imbalanced data, with each subset partitioned into k folds, where k was set to a default value of 10 (Anguita et al., 2012; Mahesh et al., 2023). This sampling strategy ensures all seven oil shales were included, and only samples with complete data for all selected training variables were utilized for the machine learning process.

The RF classifier was executed with a value of 100 estimators (i.e., number of trees in the forest) (Supplementary Fig. S1). At each tree node, the maximum number of features considered was the square root of the total number of features (Wicaksono and Lazuardi, 2018). Model performance was evaluated based on classification accuracy, specifically focusing on the true positive rate and false positive rate. The RF model identified the most important variables for partitioning the response variable in the training dataset, thereby classifying the training samples into their true categories. This process also allows for an assessment of the importance of each variable in influencing the classification accuracy. The entire RF data-processing chain was repeated 20 times to validate the stability of RF classification.

Additionally, the non-parametric Mann-Whitney test was performed on the synthesized data using *Scipy.Stats* module in Python. This test was used to identify significant differences in a given parameter between freshwater and saline lacustrine oil shales, with a significance level set at 0.05. The Mann-Whitney test results are present in Supplementary Dataset 2.

3. Results and discussion

3.1. Capacity of RF model to classify lacustrine oil shales

The RF classifier was developed to distinguish between freshwater and saline lacustrine oil shales, aiming to characterize the comprehensive differences between the two types. The confusion matrix of overall RF model demonstrates effective classification, achieving an average accuracy of 87.7 % for freshwater lacustrine oil shales and 94.9 % for saline lacustrine oil shales (Table 2). The errors observed in the RF analysis may be attributed to the high degree of similarity among certain samples. For example, oil shales from the Qingshankou Formation in the Songliao Basin are often interbedded with thin layers of siltstones exhibiting various current structures. Previous studies, including paleontological, isotopic and geochemical analyses of these rocks in the Qingshankou Formation, indicate some of these sequences were influenced by episodic seawater incursions into the lake (Hou et al., 2000; Huang et al., 2013). The shifts in geochemical indices associated with these marine incursions might have caused some shale samples to be misclassified as saline lacustrine shales.

RF classification model was also employed to assess the significance of geochemical characteristics distinguishing the two types of lacustrine oil shales studied. The importance of each variable was expressed as a percentage of mean decrease accuracy (MDA), which measures the reduction in RF prediction accuracy when the value of a variable is replaced with a random number. A higher MDA value indicates greater importance of the variable. Only the top 20 ranked geochemical variables are presented, as variables ranked lower had negligible impact on the model accuracy. Total organic content (TOC) was identified as the most important variable for classification (Fig. 2). In addition, 7 of the top 20 variables are widely used indicators of paleoproductivities,

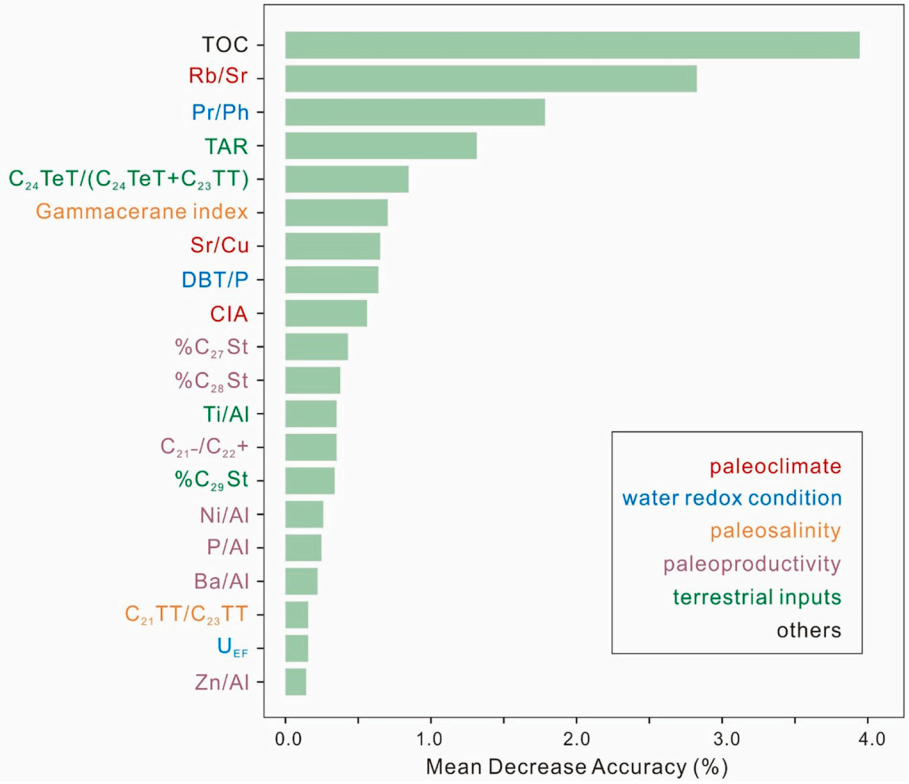

Fig. 2. Evaluation of variable importance of the random forest (RF) classification model. The "mean decrease accuracy" reflects the reduction in RF prediction accuracy when the value of a variable is replaced with a random number. A higher the value indicates greater importance of variable in the predictive performance of model. For abbreviations of parameters, see text.

including percentages of C_{27}- and C_{28} - 5α(H),14α(H),17α(H) 20R (ααα R) regular steranes relative to total ($C_{27} + C_{28} + C_{29}$) ααα R steranes (%C_{27} St and %C_{28} St), the C_{21-}/C_{22+} *n*-alkane ratio (C_{21-}/C_{22+}), and aluminum-normalized inorganic proxies, such as Ni/Al, P/Al, Ba/Al, and Zn/Al (Fig. 2; Kodner et al., 2008; Tribovillard et al., 2006; Algeo and Ingall, 2007). Among the top 20 variables, five are commonly used to indicate paleowater conditions. The pristane to phytane ratio (Pr/Ph), dibenzothiophene to phenanthrene ratio (DBT/P) and enrichment factor of uranium (U_{EF}) are used to indicate redox conditions (Hughes et al., 1995; Algeo and Tribovillard, 2009; Tribovillard et al., 2012; Ma et al., 2019) while the gammacerane index (GI = gammacerane/C_{30} hopane) and the C_{21}/C_{23} tricyclic terpane ratio ($C_{21}TT/C_{23}TT$) are used to indicate water salinity (Fig. 2; Tulipani et al., 2015; Li et al., 2021). Four proxies reflect the influxes of terrigenous OM and clastic materials into lacustrine environments: terrigenous to aquatic ratio (TAR), C_{24} tetracyclic terpane to C_{23} tricyclic terpane ratio ($C_{24}TeT/(C_{24}TeT + C_{23}TT)$), Ti/Al, and the percentage of C_{29} ααα R regular steranes relative to total ($C_{27} + C_{28} + C_{29}$) ααα R steranes (%C_{29} St) (Fig. 2; Philp and Gilbert, 1986; Murphy et al., 2000; Meyers et al., 2001; Samuel et al., 2010). Notably, three indicators of paleoclimate changes are ranked among the top 10: Rb/Sr, Sr/Cu and the chemical index of alteration (CIA) (Fig. 2; Chen et al., 1999; Goldberg and Humayun, 2010; Moradi et al., 2016).

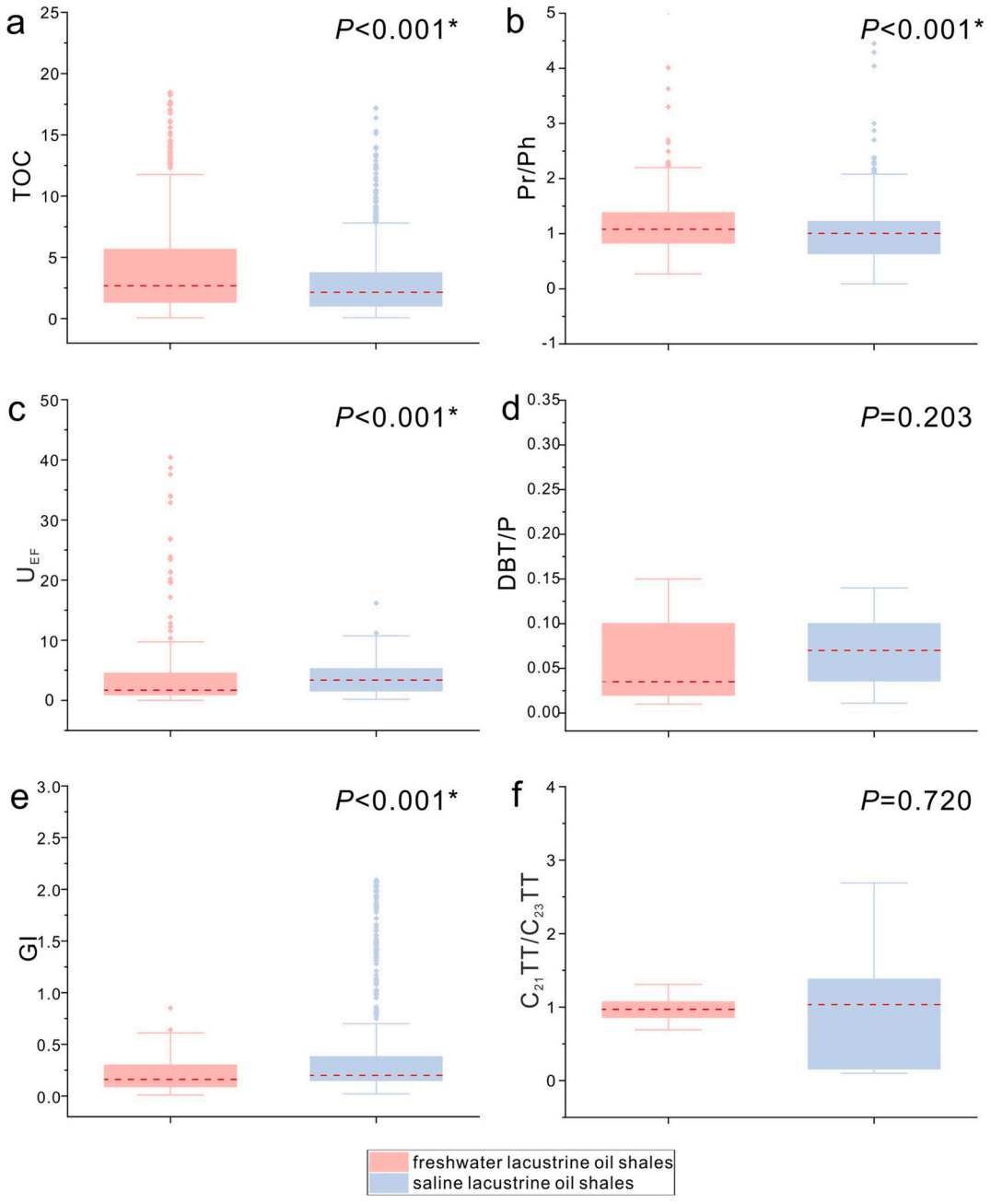

Fig. 3. Box plots comparing a) total organic carbon (TOC) content and (b–d) proxies of paleowater conditions, including (b) pristane/phytane (Pr/Ph) ratio, (c) enrichment factor of uranium (U_{EF}) (d) dibenzothiophene to phenanthrene (DBT/P) ratios, (e) gammacerane Index (GI) and (f) C_{21} tricyclic terpane/C_{23} tricyclic terpane (C_{21} TT /C_{23} TT) ratio in freshwater and saline lacustrine oil shales. Nonparametric Mann-Whitney test *P* values are shown, and asterisk indicates that a significant difference was detected ($P < 0.05$) between the freshwater and saline lacustrine oil shales. The red dashed line represents the median value. (For interpretation of the references to colour in this figure legend, the reader is referred to the web version of this article.)

3.2. Differential geochemical characteristics of freshwater versus saline water oil shales

By comparing the TOC content in the freshwater and saline lacustrine oil shales (Fig. 3a), it is evident that freshwater lacustrine oil shales are more enriched in OM relative to saline water lacustrine shales (Mann-Whitney test $P < 0.001$) (Supplementary Dataset 2). The enrichment of OM in sediments results from the interaction and coupling of various factors, and the primary mechanisms controlling the OM enrichment are input and preservation along with their interactions with each other (Schwarzkopf, 1993; Tyson, 1995). This study now investigates the mechanisms underlying the differences in TOC content between freshwater and saline lacustrine oil shales.

3.2.1. Paleowater conditions

Paleowater conditions are a key factor influencing the preservation of OM, as anoxic and stratified environments can enhance OM preservation and enrichment (Lee, 1992). Redox and salinity conditions during the shale depositions were initially determined based on biomarker ratios, including Pr/Ph, DBT/P, GI and C_{21} tricyclic terpane (TT)/C_{23} TT (Fig. 2b–f). The Pr/Ph ratio has commonly been used as indicator of redox conditions during the early diagenesis (Powell and McKirdy, 1973; Ten Haven et al., 1987; Hughes et al., 1995; Ma et al., 2019; Qiao et al., 2021), with values <1.0 typifying anoxic conditions, values between 1.0 and 2.9 suggesting suboxic settings, and values >3.0 indicating oxic environmental settings (Didyk et al., 1978; Peters et al., 2005). Here, we need to note that, aside from the source and depositional environment, organic geochemical indicators may also be influenced by maturity (Luo et al., 2020). For example, Cheng et al. (2023) found that the Pr/Ph ratio of lacustrine source rocks progressively decreases with increasing maturity. Hence, the inorganic proxy U_{EF} was used as an additional indicator to examine the redox conditions of the depositional environment. Under oxidizing conditions, U is typically present in water as dissolved U^{6+}, whereas U^{6+} is transformed into insoluble U^{4+} under anoxic conditions and becomes enriched in sediments (Skomurski et al., 2011; Algeo and Tribovillard, 2009). The enrichment factor of U has been widely to assess the redox conditions, and U_{EF} greater than 1 indicates that U is enriched relative to their average crustal abundance, suggesting an anoxic environment (Tribovillard et al., 2006; Algeo and Tribovillard, 2009; Sweere et al., 2016; Lu et al., 2021; Zirks et al., 2021). Both freshwater and saline lacustrine oil shales exhibit Pr/Ph ratios around 1 and U_{EF} values greater than 1, indicating that both types of oil shales were deposited in anoxic lacustrine environments. Compared to freshwater lacustrine oil shales, the saline lacustrine oil shales exhibit significantly lower Pr/Ph ratios and higher U_{EF} values (Fig. 3b and c), reflecting more reducing conditions in the saline paleolakes than freshwater paleolakes. DBT, a sulfur-containing compound widely found in oils and ancient sediments, is commonly used to assess the depositional environment of shales (Hughes et al., 1995; Fan et al., 1991; Li et al., 2013; Zhang et al., 2021a). DBT formation is mostly associated with reducing conditions, low ferrous ion concentrations, and high sulfate levels (Hughes et al., 1995). Although the DBT/P ratio was identified as an important factor in the RF analysis, the Mann-Whitney test results show no statistically significant difference in the DBT/*P* values between freshwater and saline lacustrine oil shales (Fig. 3d), indicating that the DBT/P ratio alone cannot differentiate between the two types of lacustrine oil shales in China.

Changes in water salinity within a lake are key factors influencing the stratification of the water column and the formation of anoxic conditions at the lake bottom (Sinninghe Damsté et al., 1995; Wang et al., 2011). In this study, two proxies associated with salinity, GI and C_{21} TT/C_{23} TT ratio, rank among the top 20 important proxies in the RF classification (Fig. 2). High GI value has been widely used to indicate a stratified water column in both marine and non-marine depositional environments, typically resulting from hypersalinity at depth (Moldowan et al., 1985; Fu et al., 1986; Philp et al., 1991). Alternatively, gammacerane may originate from bacterivorous ciliates inhabiting the chemocline within the water column, suggesting that high concentrations of gammacerane can also reflect a well-stratified water column, even in the absence of high-salinity bottom waters (Sinninghe Damsté et al., 1995; Schwark et al., 1998). In our study, significantly higher GI values were observed in saline lacustrine oil shales than freshwater lacustrine oil shales (Fig. 3e), indicating a more saline and salinity-driven stratification in saline lacustrine basins. This finding aligns with previous studies that reconstruct salinity conditions based on lithological associations. As salinity increases in lacustrine basins, Ca—Mg carbonate minerals, such as calcite, aragonite, and dolomite, begin to precipitate, marking the primary stage of salinization in the lake (Warren, 2016). In China, saline lacustrine deposits are typically characterized by carbonate-rich shales, while freshwater lacustrine deposits are predominantly composed of siliceous and clay-rich rocks, which are generally carbonate-poor (Li et al., 2022a). These the differences reflect variations in aquatic conditions during the deposition of these two types of lacustrine oil shales. In addition, the C_{21}TT/C_{23}TT ratio appears to decrease with elevated salinity of the depositional water. This ratio was developed based on the observations that TTs typically show a predominance of the C_{23}TT in marine facies and a dominance of the C_{21}TT in freshwater lacustrine facies (Peters et al., 2005). However, our Mann-Whitney tests reveal no significant difference in the C_{21}TT/C_{23}TT ratio between freshwater and saline lacustrine oil shales (Fig. 3f). Furthermore, the C_{21}TT/C_{23}TT ratios in saline lacustrine oil shales vary in a wide range, with some samples exhibiting higher values than freshwater ones (Fig. 3f). Considering that the exact precursors of the TTs have not been fully identified (Dutta et al., 2006; Philp et al., 2021), we propose that salinity was not the sole factor influencing the distribution of the C_{21}TT/C_{23}TT ratios in the two types of lacustrine oil shales. For example, elevated inputs of planktonic OM can lead to a predominance of the C_{23}TT over the C_{21}TT, while increased input of terrigenous plants-derived OM may result in a predominance of the C_{21}TT over the C_{23}TT (Wang et al., 2023a, and references therein). Therefore, we call for future studies to incorporate multiple proxies when reconstructing the salinity of depositional environments, rather than relying solely on the C_{21}TT/C_{23}TT ratio as an indicator of salinity.

In summary, compared to freshwater lacustrine basins, saline lacustrine basins are associated with more reducing and stratified environments, which generally favor the enrichment of OM in sediments. Despite this, saline lacustrine oil shales exhibit lower TOC content. This observation suggests that paleowater conditions alone did not account for the differences in TOC content between the freshwater and saline lacustrine oil shales. Other factors must be contributing to the variations in OM contents observed in these environments.

3.2.2. Paleoproductivity

The input of OM is mainly controlled by primary productivity (Katz, 2005). Lacustrine primary productivity levels were assessed using molecular biomarker-derived ratios, i.e., %C_{27} St and %C_{28} St and C_{21-}/C_{22+}, and elemental geochemical indicators, i.e., major element P and trace metals Ni, Ba and Zn. C_{27} and C_{28} steranes serve as biomarkers for productivity, particularly for red and green algae, respectively (Kodner et al., 2008). The C_{21-}/C_{22+} ratio represents the sum of C_{14}–C_{20} *n*-alkanes relative to the sum of C_{23}–C_{33} *n*-alkanes, where short-chain *n*-alkanes (<C_{21}) are typically abundant in algae and microorganisms, while long-chain homologues (>C_{22}) are generally associated with terrigenous higher plant (Eglinton and Hamilton, 1967; Cranwell et al., 1987; Ficken et al., 2000; Lu and Meyers, 2009). Compared to saline lacustrine oil shales, freshwater lacustrine oil shales have higher percentages of C_{27} steranes relative to total steranes (%C_{27} St) and higher C_{21-}/C_{22+} values (Fig. 4a and c, Supplementary Dataset 2). The relative abundances of C_{28} steranes (%C_{28} St) in saline lacustrine oil shales were significantly higher than in freshwater lacustrine shales (Fig. 4b). This finding aligns with our expectations, as green algae community has been characterized

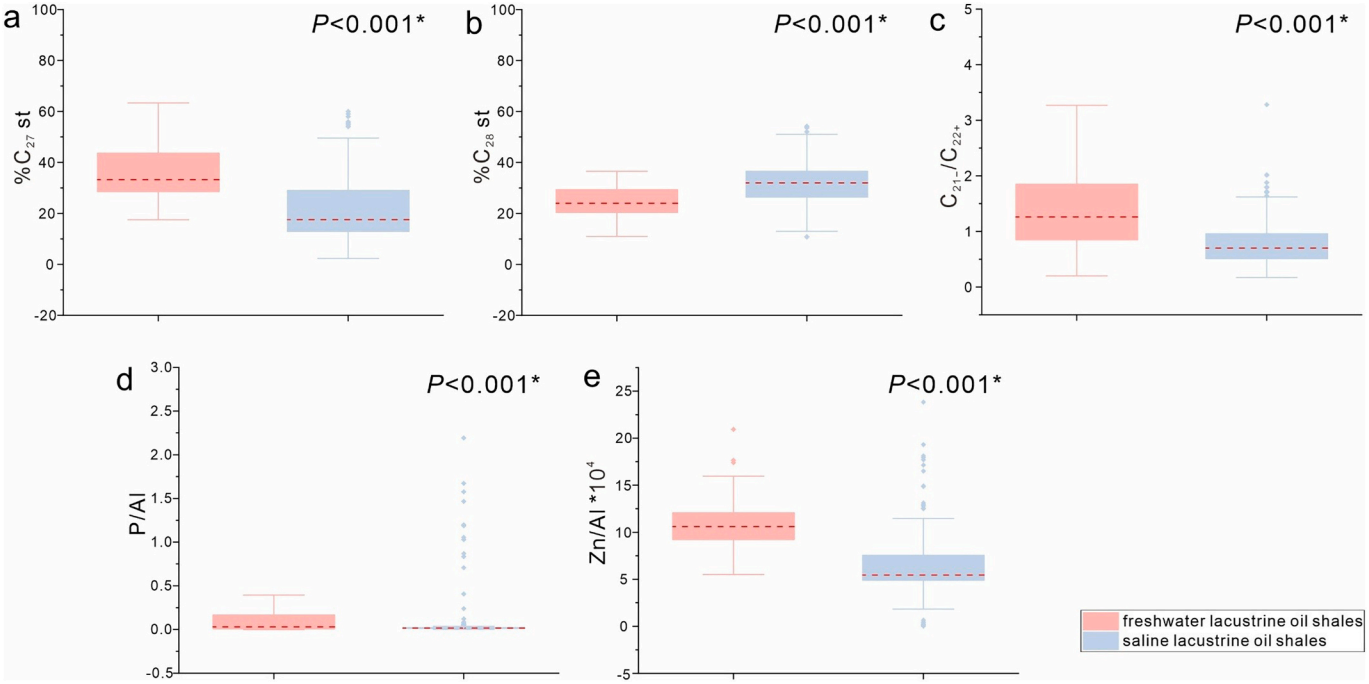

Fig. 4. Box plots comparing paleoproductivity indicators in freshwater and saline lacustrine oil shales: a) percentage of C_{27} steranes relative to the total concentrations of C_{27}, C_{28}, and C_{29} steranes (%C_{27} St), b) percentage of C_{28} steranes relative to the total concentrations of C_{27}, C_{28}, and C_{29} steranes (%C_{28} St), c) C_{21-}/C_{22+} *n*-alkane ratio (C_{21-}/C_{22+}), d) P/Al ratios and e) Zn/Al ratios. Nonparametric Mann-Whitney test *P* values are shown, and asterisk indicates that a significant difference was detected ($P < 0.05$) between the freshwater and saline lacustrine oil shales. The red dashed line represents the median value. For abbreviations of parameters, see text. (For interpretation of the references to colour in this figure legend, the reader is referred to the web version of this article.)

as "disaster species" due to their strong survival capability in oxygen-depleted and high-salinity conditions, which are unfavorable for most other photoautotrophic plankton species (Tappan, 1980; Schwark and Empt, 2006). As such, the high content of C_{28} steranes have been documented in shales from various saline lacustrine basins, including the Green River shale, the shales of the Fengcheng and Lucaogou formations, and first member of Shahejie Formation (Horsfield et al., 1994; Meng et al., 2011; Gao et al., 2016; Cao et al., 2020).

In addition to biomarker proxies, higher total productivities in freshwater paleolakes are also supported by elevated P/Al, Ni/Al, Zn/Al, and Ba/Al ratios in the freshwater lacustrine shales compared to their saline counterparts (Fig. 4d and e, Supplementary Dataset 2). Element P, a critical constituent of organisms, is often preserved in sediments following the decomposition of organic material, and may later form autogenous phosphate minerals (Redfield, 1958; Schenau et al., 2005; Algeo and Ingall, 2007). Ni, Zn and Ba have been widely used to assess paleoproductivity, particularly under anoxic conditions, as these elements are delivered to sediments primarily in the form of organometallic complexes associated with organic matter and are less influenced by redox conditions (Tribovillard et al., 2006; Bejugam and Nayak, 2019). The higher values of productivity-derived ratios in the freshwater lacustrine shales indicate greater overall productivity in these lakes, resulting in increased OM production and subsequent enrichment in the sediments. The lower paleoproductivity in the saline water lake is expected, as high salinity can inhibit the activities of algae, plankton and zooplankton, reducing OM production, and, consequently, OM accumulation in the sediments.

It is noteworthy that the bottom water environment of freshwater lacustrine basins is characterized by less reducing environments relative to saline lacustrine basins, combined with substantial inputs of algae and plankton. This could result in active aerobic microbial processes both in the ancient lake water column and at the lake bottom. Evidence of such microbial activity has been found in freshwater-deposited Chang 7 oil shales, including abundant carbonate concretions and microfossils of microbial mats (Zhu et al., 2020b; Liu et al., 2022). Additionally, findings of abundant microbial degradation-derived bituminite macerals and bacteria-derived biomarkers (e.g., 3β-methylhopanes) in the freshwater-deposited Qingshankou Formation further support this viewpoint (Zhu et al., 2020a; Wang et al., 2023b). However, the higher TOC content in freshwater lacustrine oil shales indicates that the primary production of algae and phytoplankton in the ancient lake was sufficient to surpass the degradation of OM by microorganisms in the water column, leading to greater accumulation of OM in sediments.

High primary productivity is a fundamental factor in the formation and development of source rocks (Tissot and Welte, 1984). In marine sedimentary environments, high primary productivity has been observed in modern continental margins, where upwelling currents and enhanced terrigenous inputs bring nutrient-rich waters to the surface, leading to prolific phytoplankton blooms (Pedersen and Calvert, 1990; Caplan and Bustin, 1999; Gallego-Torres et al., 2007). This results in substantial OM input to the seafloor, even in sediments subject to significant bioturbation, where high OM preservation can still occur. Consequently, high surface water productivity is considered as a major controlling factor for OM enrichment and preservation in marine sediments (Pedersen and Calvert, 1990; Gallego-Torres et al., 2007). Some researchers argue that, in the context of marine sedimentary environments, high surface productivity is more crucial than anoxic bottom waters for OM enrichment (Pedersen and Calvert, 1990; Sageman et al., 2003; Shi et al., 2018). Our results indicate a similar process in paleolakes and supports the notion that high productivity may be a key mechanism contributing to the differences in OM abundance between freshwater and saline lacustrine oil shales.

3.2.3. *Terrigenous influxes*

Three biomarker indicators of terrigenous OM inputs that rank among the top 20 most important parameters for the RF classification (Fig. 2). TAR, defined as $(nC_{27} + nC_{29} + nC_{31})/(nC_{15} + nC_{17} + nC_{19})$, reflects the relative input of terrigenous versus aquatic OM, with higher

values indicating a greater contribution from higher plants (Cranwell et al., 1987; Bourbonniere and Meyers, 1996). Most samples, whether from freshwater or saline lacustrine oil shales, have TAR ratios below 1 (Fig. 5b), indicating that contributions from terrigenous OM were less than those from aquatic sources in both types of shales. C_{29} steranes are commonly used as a proxy for vascular plant input, with the caveat that some diatoms, cyanobacteria and algae are also potential sources (Patterson, 1971; Moldowan et al., 1985; Kodner et al., 2008; Ding et al., 2024). C_{24} tetracyclic terpane (TeT) can be produced via microbial-mediated decyclization of the *E*- or A-rings of terrigenous triterpenes (Woodhouse et al., 1992; Samuel et al., 2010). The ratios of C_{24}TeT and C_{23}TT and the proportion of C_{29} steranes relative to total steranes (%C_{29} St) are often used to indicate terrigenous OM inputs, particularly from higher plants (Philp and Gilbert, 1986). In saline lacustrine oil shales, higher values of TAR, $C_{24}TeT/(C_{24}TeT + C_{23}TT)$ and %C_{29} St (C_{29} ααα*R* steranes/(C_{27} + C_{28} + C_{29}) ααα*R* steranes ×100 %) (Fig. 5a, b and c; Supplementary Dataset 2) indicate stronger terrigenous OM input into saline lakes. It is important to note that the biomarker proxies used here represent the relative contributions of terrigenous OM compared to aquatic OM. Therefore, the elevated ratios observed in saline lacustrine oil shales may be due to reduced aquatic OM input, which is likely a consequence of lower productivity associated with high salinity conditions.

In this study, the strength of terrigenous inputs into lakes was also assessed using inorganic geochemical proxies, such as Ti/Al and SiO_2/Al_2O_3 ratios (Fig. 5d and e). The Ti/Al ratio is extensively used as a proxy to indicate detrital influx (Rimmer, 2004; Tribovillard et al., 2006; Lash and Blood, 2014), where Al mainly originates from aluminosilicate clay minerals in fine-grained sediments while Ti is enriched in the sand- and silt-sized grains, such as ilmenite and rutile (Young and Nesbitt, 1998; Caplan and Bustin, 1999; Calvert and Pedersen, 2007). Ti/Al ratio ranks among the top 20 most important parameters for RF classification, with higher Ti/Al ratios indicating a greater influx of detrital sediments (Walker et al., 1988). Although the SiO_2/Al_2O_3 ratio was only listed as top 20 proxies by RF analysis, but was included for Mann-Whitney test as a proxy for detrital influx. The aluminum-normalized Si ratio represents the proportion of quartz to aluminosilicate minerals in the sediments (Murphy et al., 2000) and has been widely used as terrestrial proxies (Ross and Bustin, 2009; Xu et al., 2018; Hofer et al., 2013). Since silica can originate from biogenic sources such as diatoms, silicoflagellates, and radiolarians (Gehlen et al., 2002), we evaluated the potential source of SiO_2 by examining the relationship between SiO_2 and Al_2O_3. In the studied oil shales, SiO_2 and Al_2O_3 are positively correlated (Spearman's $\rho = 0.471$, $P < 0.001$), indicating that silica likely originated from clay minerals. Consequently, the higher Ti/Al and SiO_2/Al_2O_3 ratios in the saline lacustrine oil shales (Fig. 5 d and e) suggest greater terrigenous detrital inputs into saline basins, which may have diluted the OM in the sediments, leading to lower TOC contents. Furthermore, both Ti and Si are preserved in high-density, coarser-grained sediments, making aluminum-normalized Ti and Si useful proxies for high-energy environments, such as shallow water settings (Algeo and Maynard, 2004; Ross and Bustin, 2009). Thus, the elevated Ti/Al and SiO_2/Al_2O_3 ratios in the saline lacustrine oil shales reflect lower lake levels of saline basin relative to freshwater lakes, enabling more detrital influx to reach the depositional sites. In contrast, the studied freshwater lacustrine oil shales were deposited in deeper lake basins, consistent with previous findings. Earlier studies have suggested that oil shales of the Chang 7 and Qingshankou formations formed in semi-deep to deep lake facies during periods when the paleolakes in the Ordos and Songliao basins reached their peak expansion (Jia et al., 2013a; Li et al., 2017; Liu et al., 2017a).

Terrigenous influxes play a crucial role in OM enrichment. On one hand, they supply essential biological nutrients, promoting the production of OM; on the other hand, they can dilute the concentration of OM (Hupp and Weislogel, 2018). Our results indicate that the low-TOC saline lacustrine shales contain elevated inputs of terrigenous OM and detrital sediments compared to the freshwater shales. This implies that the primary role of terrigenous influx was not to boost paleoproductivity by supplying nutrients, but rather to dilute OM in the saline lacustrine basins. In contrast, increased lake depth in freshwater lacustrine basins

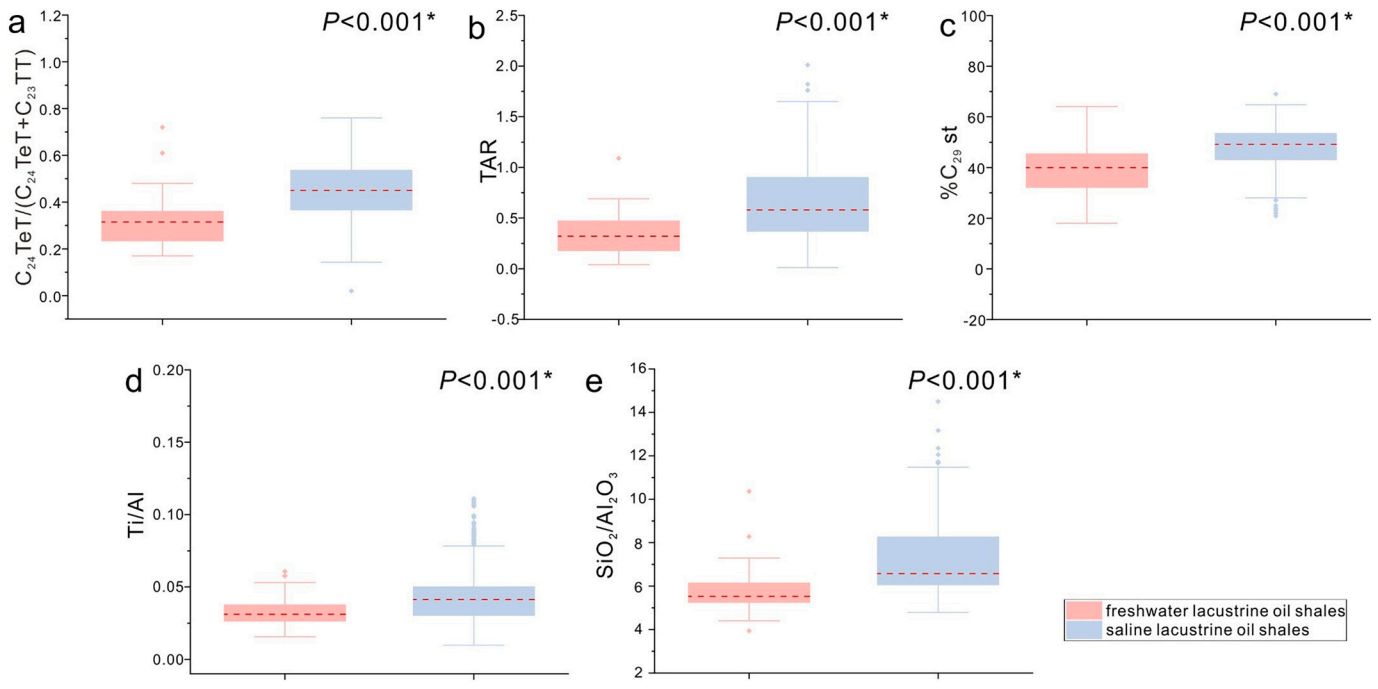

Fig. 5. Box plots comparing terrestrial input indicators in freshwater and saline lacustrine oil shales: a) C_{24} tetracyclic terpanes to C_{23} tricyclic terpanes ratio ($C_{24}TeT/(C_{24}TeT + C_{23}TT)$); b): terrigenous to aquatic ratio (TAR), c) percentage of C_{29} steranes relative to the total concentrations of C_{27}, C_{28}, and C_{29} steranes (% C_{29} St), d) Ti/Al ratio, and e) SiO_2/Al_2O_3 molar ratio. Nonparametric Mann-Whitney test *P* values are shown, and asterisk indicates that a significant difference was detected ($P < 0.05$) between the freshwater and saline lacustrine oil shales. The red dashed line represents the median value. (For interpretation of the references to colour in this figure legend, the reader is referred to the web version of this article.)

may inhibit mixing between surface and bottom waters. As the water depth of freshwater lakes increased, a large, restricted basin formed, reducing terrigenous influx and mixed sediment deposition. This might create a quiet bottom-water environment conducive to OM preservation, ultimately leading to OM enrichment in sediments and thus higher TOC contents.

3.2.4. Paleoclimate

Three weathering-sensitive elemental ratios, i.e., Rb/Sr, Sr/Cu and CIA, rank among the top 10 most important proxies in the RF analyses (Fig. 6), underscoring the significance of climatic variations in distinguishing between freshwater and saline lacustrine oil shales. Chemical weathering on continents is primarily influenced by moisture and temperature levels (Nesbitt and Young, 1982; Sheldon and Tabor, 2009). The CIA serves as a proxy for the degree of chemical weathering in soils and sediments, with implications for paleoclimate reconstruction (Lu et al., 2021; Chen et al., 2017; Sun et al., 2022; Liu et al., 2024). Higher CIA values are associated with increased removal of mobile cations during chemical weathering, which is more pronounced in warmer and wetter climates (Nesbitt and Young, 1989; Wang et al., 2020). Rb and Cu are relatively stable and more resistant to weathering, while Sr tends to be depleted under warm and humid conditions (Lerman et al., 1995), contributing to increased Rb/Sr values and decreased Sr/Cu values (Chen et al., 2001; Lv et al., 2022). In this study, the freshwater lacustrine oil shales have higher CIA and Rb/Sr values but lower Sr/Cu ratios compared to saline lacustrine oil shales, suggesting that the freshwater lacustrine oil shales were deposited under warmer and wetter climatic conditions. These findings align with previous sedimentary studies, which show that sediments in freshwater lacustrine deposits are largely composed of marls, fine-grained sandstones, and siltstones, reflecting a wet climate during the deposition (Zou et al., 2019, and references therein). In contrast, saline and brackish lacustrine deposits are typically characterized by clastic and carbonate rocks, with intense dolomization observed in salt-water-deposited oil shales (Zou et al., 2019, and references therein), indicative of a drier climatic condition.

We compared the depositional intervals of studied seven lacustrine oil shales with global trends in atmospheric CO_2 levels (Foster et al., 2017), atmospheric temperatures (Scotese et al., 2021), and precipitation levels (Li et al., 2022b) throughout the Phanerozoic (Fig. 7a). Additionally, we note that other lacustrine oil shales in China and worldwide have also been mined (Zou et al., 2019; Dyni, 2003) (Fig. 7b, Table 1). Our results reveal that freshwater lacustrine oil shales were predominantly deposited during periods characterized by high atmospheric CO_2 or increasing CO_2 trends with high precipitation, corresponding to greenhouse periods or warmer intervals within icehouse periods (Fig. 7). Elevated surface air temperature can increase atmospheric water vapor, resulting in a humid climate with high precipitation, conducive to the formation of freshwater lakes. Conversely, synthesized saline lacustrine oil shales were primarily deposited during periods of low atmospheric CO_2 levels or decreasing CO_2 trends, typical of icehouse conditions with reduced precipitation (Fig. 7). Decreased surface air temperature could reduce atmospheric water vapor, fostering a drier climate that favored the formation of saline lakes. These distinctions highlight the significant influence of CO_2-induced long-term climate variations on lacustrine depositional environments. Due to the absence of comprehensive geochemical data, these additional lacustrine oil shales were not included into the RF analysis but were referenced for comparisons with long-term climate shifts. However, the impact of climate on OM enrichment in different types of lacustrine oil shales has been acknowledged by previous studies based on analyses of lacustrine oil shales from single basins. For example, Walters et al. (2020) and

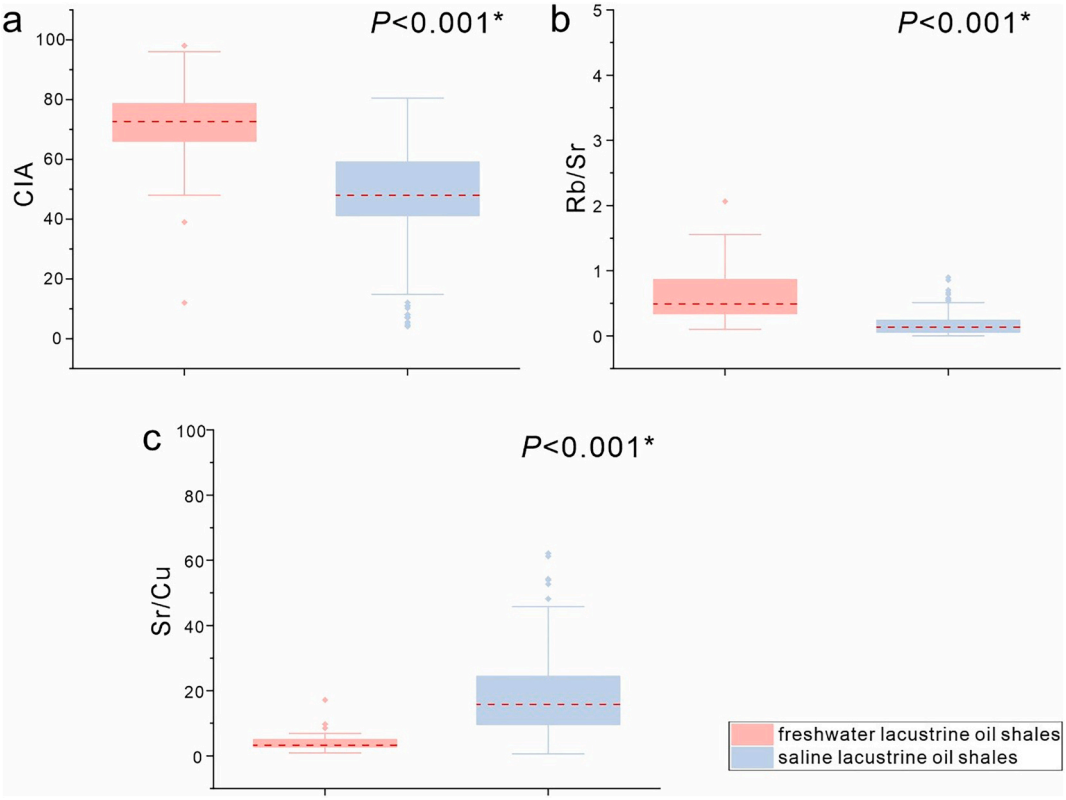

Fig. 6. Box plots comparing paleoclimate conditions during the deposition of freshwater and saline lacustrine oil shales. a) Chemical index of alteration (CIA), b) Rb/Sr ratio, and c) Sr/Cu ratio. Nonparametric Mann-Whitney test *P* values are shown, and asterisk indicates that a significant difference was detected ($P < 0.05$) between the freshwater and saline lacustrine oil shales. The red dashed line represents the median value. (For interpretation of the references to colour in this figure legend, the reader is referred to the web version of this article.)

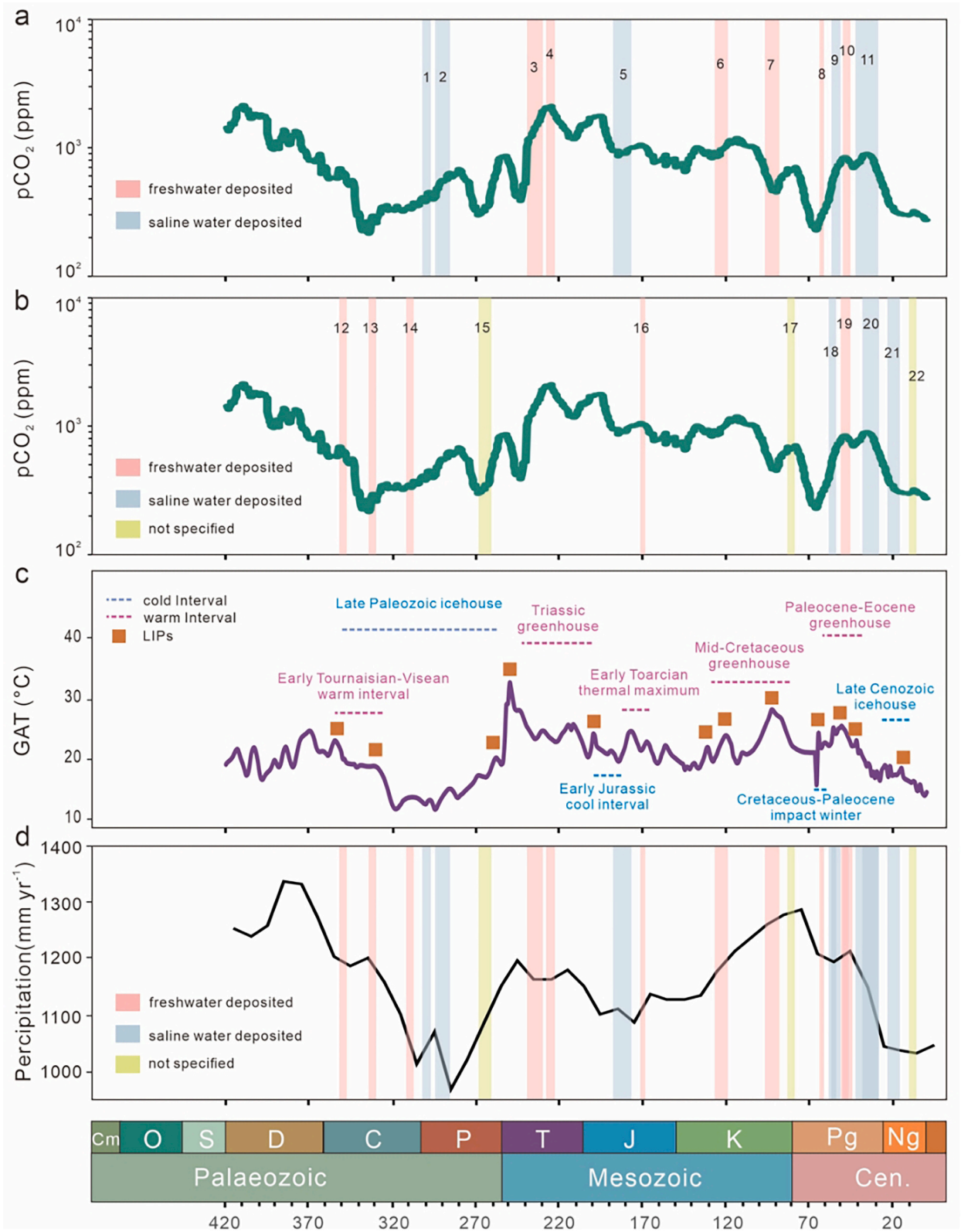

Fig. 7. Comparisons of paleoclimate evolutionary patterns throughout the Phanerozoic and the occurrences of major lacustrine oil shales in China and globally. Numbers in Panels (a) and (b) represent the major lacustrine oil shales in China and other regions of the world. Panel (a) is for oil shales 1–11, and (b) is for 12–22. The names and numbers are summarized in Table 1. The atmospheric CO_2 level curves in panels (a) and (b) are from Foster et al. (2017). Panel (c) represents global atmospheric temperature (GAT; Scotese et al., 2021). The duration of warm and cool time intervals and timings of Large Igneous Province (LIPs) eruptions are based on Scotese et al. (2021). Panel (d) illustrates precipitation trends (Li et al., 2022b). Blue bands mark the depositional intervals of freshwater lacustrine oil shales, pink bands outline the depositional intervals of saline lacustrine oil shales, and yellow-green bands indicate lacustrine oil shale intervals where the type of basin is unspecified. (For interpretation of the references to colour in this figure legend, the reader is referred to the web version of this article.)

Table 1
Spatiotemporal distributions of major lacustrine oil shales in China and other regions of the world.

No.*	Text_age	Num_age (Ma)	Location (country, region/province/state /basin)	Stratigraphy	Type of lacustrine type	References
1	Early Permian (Kasimovian to Asselian)	300	China, Junggar Basin	Fengcheng Formation	Saline	Yu et al. (2019); Wang et al. (2022)
2	Early Permian	294–286.1	China, Jimsar Sag of Junggar Basin	Lucaogou Formation	Saline	Ding et al. (2019); Sun et al. (2022)
3	Middle–Late Triassic (Ladinian)	237–227	China, Ordos Basin	Chang 7 oil shales of Yanchang Formation	Freshwater	Yang and Zhang (2005); Li et al. (2017); Bai and Ma (2020); Zhang et al. (2021b)
3	Late Triassic (Carnian)	235	China, Junggar Basin	Baijiantan Formation	Freshwater	Stevens et al. (2013); Gao et al. (2017); Zheng et al. (2017)
4	Late Triassic (Norian to Rhaetian)	227	China, Sichuan Basin	Xujiahe Formation (gas source rock)	Freshwater	Deng et al. (2019); Huang (2019)
5	Early Jurassic (late Pliensbachian to the early Aalenian)	186	China, Junggar Basin	Sangonghe Formation	Freshwater	Huang (2019); Qiao et al. (2023); Li et al. (2024b)
5	Early Jurassic (late Pliensbachian to Toarcian)	185–174	China, Sichuan Basin	Ziliujing Formation	Freshwater	Zhang et al. (2011); Li et al. (2024a)
6	Early Cretaceous	135–121	China, Erlian Basin	Bayanhua Group	Saline	Luo et al. (2018); Guo et al. (2018); Wu et al. (2023)
7	Late Cretaceous (Cenomanian–Turonian, TOAE2)	100–88	China, Songliao Basin	Qingshankou Formation	Saline	Jia et al. (2013b); He et al. (2019)
8	Paleocene	60–58	China, Subei Basin	Second member of Funing Formation	Saline to Freshwater	Duan et al. (2020); Zhu et al. (2023)
9	Paleocene to Eocene	55–50.5	China, Bohai Bay Basin	Kongdian Formation	Saline	Liu et al. (2017b); Fang et al. (2022)
10	Middle Eocene (Lutetian)	45–42	China, Fushun Basin	Jijuntun Formation	Freshwater	Hong et al. (1980); Meng et al. (2012); Strobl et al. (2014); Xu et al. (2016)
10	Late Eocene	37.5–35.5	China, Qaidam Basin	Upper member of Xiaganchaigou Formation	Saline	Zhao et al. (2019); Zhang et al. (2023)
10	Middle Eocene (Lutetian to Bartonian)	48–38	China, Maoming Basin	Youganwo Formation	Freshwater	Herman et al. (2017); Xu et al. (2022)
11	Eocene to Oligocene	43–32.8	China, Bohai Bay Basin	Shahejie Formation	Saline	Liu et al. (2017b); Yin et al. (2020)
11	Eocene to Oligocene	43–30	China, Jianghan Basin	Qianjiang Formation	Saline	Xu (1995); Li et al. (2018); Zheng et al. (2021)
12	Early Carboniferous	350–345	Canada, Nova Scotia, Antigonish Basin	Big Marsh oil shale of Rights River Formation	Freshwater	Smith et al. (1991); Mukhopadhyay et al. (1998); Goodarzi et al. (2019a); Goodarzi (2020b)
12	Early Carboniferous	350–345	Canada, New Brunswick	Albert Formation oil shales	Freshwater	Smith et al. (1991); Mukhopadhyay et al. (1998); Goodarzi et al. (2019b); Goodarzi (2020b)
13	Early to Middle Carboniferous (Mississippian)	335–330	Canada, Newfoundland, Deer Lake Basin	Deer lake oil shales	Not specified	Hyde (1984); Wright et al. (1996)
13	Early to Middle Carboniferous (Mississippian)	335–330	Canada, Nunavut, Ontario, Sverdrup Basin	Oil shale of Emma Fiord Formation	Freshwater	Davies and Nassichuk (1988); Embry and Beauchamp (2008); Goodarzi (2020a); Goodarzi et al. (2021)
14	Late Carboniferous	309–306	Canada, Nova Scotia, Stellarton Basin	Oil shales in Stellarton Formation	Freshwater	Bell (1958); Smith et al. (1991); Yawanarajah and Kruge (1994); Mukhopadhyay et al. (1998); Lyons et al. (1995)
15	Late Permian	280	Australia, Queensland, Alpha	N.A.	Not specified	Gibson (1980); Gibson (1989);
16	Middle Jurassic–Early Cretaceous	165–158	Mongolia, Khootiin Khotgor area	Oil shale of Eedemt Formation	Freshwater	Avid and Purevsuren (2001); Ando et al. (2011); Li et al. (2014); Hasegawa et al. (2018); Erdenetsogt et al. (2022)
17	Late Cretaceous	82–78	Morocco, Timahdit	N.A.	Not specified	Kribii et al. (2001)
18	Paleocene to Eocene	50–48	Turkey, Bolu	Hatildag oil shales	Saline	Taka and Şener (1988); Sari and Aliyev (2005); Guelbay and Korkmaz (2008)
18	Eocene	53.5–48.5	United States, Colorado, Utah and Wyoming	Green River Formation	Saline to Freshwater	Surdam and Stanley (1979); Smith et al. (2003); Rosenberg et al. (2015)
19	Early Middle Eocene	50	Australia, Queensland, Byfield	N.A.	Freshwater	Gibson (1980); Gibson (1989); Knaus et al. (2010); Glikson-Simpson (2021)
19	Early Middle Eocene	50	Australia, Queensland, Condor	N.A.	Freshwater	Gibson (1980); Green and Bateman (1981); Dixon and Pope (1987); Hutton (1988); Gibson (1989); Knaus et al. (2010); Glikson-Simpson (2021)
19	Middle to Late Eocene	45	Australia, Queensland, Duaringa Basin	Duaringa Formation	Freshwater	Gibson (1980); Gibson (1989); Knaus et al. (2010); Glikson-Simpson (2021)
19	Early Middle Eocene	50	Australia, Queensland, Herbert Creek Basin	N.A.	Freshwater	Gibson (1980); Gibson (1989); Knaus et al. (2010); Glikson-Simpson (2021)

(*continued on next page*)

Table 1 (*continued*)

No.*	Text_age	Num_age (Ma)	Location (country, region/province/state /basin)	Stratigraphy	Type of lacustrine type	References
19	Middle to Late Eocene	45	Australia, Queensland, Lowmead Basin	Lowmead Formation	Freshwater	Gibson (1980); Dixon and Pope (1987); Gibson (1989); Knaus et al. (2010); Glikson-Simpson (2021)
19	Early Miocene	55	Australia, Queensland, Mount Coolon	N.A.	Freshwater	Gibson (1980); Gibson (1989); Knaus et al. (2010); Glikson-Simpson (2021)
19	Early Middle Eocene	50	Australia, Queensland, Nagoorin Graben	N.A.	Freshwater	Gibson (1980); Gibson (1989); Knaus et al. (2010); Glikson-Simpson (2021)
19	Early Middle Eocene	50	Australia, Queensland, Rundle	N.A.	Freshwater	Gibson (1980); Gibson (1989); Knaus et al. (2010); Glikson-Simpson (2021)
19	Early Middle Eocene	50	Australia, Queensland, Stuart	N.A.	Freshwater	Gibson (1980); Gibson (1989); Knaus et al. (2010); Glikson-Simpson (2021)
19	Early Middle Eocene	50	Australia, Queensland, Yamba	N.A.	Freshwater	Gibson (1980); Gibson (1989); Knaus et al. (2010); Glikson-Simpson (2021)
20	Oligocene	32	Brazil, Sao Paulo, Paraíba Valley	Paraiba valley oil shales	Freshwater	Abreu (1949); Padula (1969); Zimmerle (1985); Loureiro and Cardoso (1990)
20	Oligocene	33–25	Turkey, Bilecik	Golpazari oil shales	Saline	Yanilmaz et al. (1980); Altun et al. (2006); Guelbay and Korkmaz (2008)
20	Late Eocene to Early Oligocene	37	United States, Nevada	Elko Formation	Saline	Moore et al. (1983); Johnson et al. (2016)
21	Middle to Late Miocene	12.5	Turkey, Ankara	Beypazari oil shales	Saline	Şener et al. (1995); Altun et al. (2006); Guelbay and Korkmaz (2008); Ocakoğlu et al. (2012); Ş ener et al. (2013)
21	Middle to Late Miocene	21–19	Turkey, Kutahya	Seyitomer oil shales	Saline	Şener and Şengüler (1992); Sari and Aliyev (2005); Altun et al. (2006); Guelbay and Korkmaz (2008)
22	Late Miocene to Pliocene	10–8	Thailand, Tak	Mae Sot oil shales	Freshwater	Brown (1951); Endo (1966); Curiale and Gibling (1994); Suwannathong and Khummongkol (2007)

* The numbers correspond to those in Figs. 7 and 8. The localities of the oil shales are shown in Fig. 1.

Birgenheier et al. (2019) proposed that altering climate changes during the early Eocene influenced the OM enrichment in the Green River Formation. They suggested that when climate was relatively drier, overall salinity increased, causing the chemocline to rise. As a result, organic-rich sediments were more likely to be preserved due to reduced oxygen availability below the chemocline, facilitating the formation of saline lacustrine oil shales in the Green River Formation.

Moreover, we examined the paleo-latitudinal distribution of synthesized lacustrine oil shales (Fig. 8). Latitude is key for climate classification as it governs solar radiation, temperature, and atmospheric circulation patterns (Barry and Chorley, 2009; Cui et al., 2021). According to the climate classification by Boucot et al. (2013) and Scotese (2016), 28.6 % of compiled freshwater lacustrine oil shales were deposited in a warm temperate zone, followed by 25.0 % in tropical and subtropical zones. In the modern world, annual atmospheric temperatures range from <18 °C to >22 °C for a warm temperate zone and 20–30 °C for tropical and subtropical zones, both of which are characterized by abundant rainfall (Trewartha and Horn, 1980). These conditions provide ample freshwater inputs necessary for the formation of freshwater lacustrine basins. In contrast, 17.9 % of saline water lacustrine shales were found in arid zones characterized by low precipitation and high evaporation, favoring the formation of saline lakes (Trewartha and Horn, 1980). Interestingly, 17 % of saline lacustrine shales occurred in tropical and subtropical zones, known for high precipitation. The dispersion in latitude distribution suggests that latitudinal climatic differences may not be the primary factor influencing the differential formations of freshwater and saline paleolakes.

Table 2
True positive rates (TPR) and false positive rates (FPR) of the Random Forest classifier trained on freshwater and saline lacustrine oil shales. Mean values and twice standard error of the mean (2SEM) were calculated from resampling calculations.

Setting	TPR_mean (%)	TPR_2SEM (%)	FPR_mean (%)	FPR_2SEM (%)
Freshwater lacustrine oil shales	87.7	0.8	12.4	0.9
Saline lacustrine oil shales	94.9	0.4	5.2	0.4

3.3. Climate-driven differences in OM enrichment patterns

Our results indicate that climate significantly influenced the differential OM enrichment patterns in freshwater versus saline water lacustrine oil shales in China. This influence was exerted through the regulation of primary productivity, paleowater conditions, terrigenous influxes and geochemical characteristics of sediments deposited in these lacustrine environments. In this study, we propose a climate-driven model explaining the differing patterns of OM enrichment in freshwater and saline lacustrine basins (Fig. 9).

During the depositions of freshwater lacustrine oil shales, variations in CO_2 levels led to a humid and warm climate. High annual precipitation and reduced evaporation facilitated lake expansion by increasing river discharge and freshwater input. This influx lowered lake salinity and reduced stratification, creating a stable bottom-water environment favorable for OM accumulation and preservation. Algae and phytoplankton blooms during the humid and warm climate generated substantial amounts of OM, with the primary supply derived from aquatic sources. Additionally, the humid and warm conditions promoted the growth of terrigenous plants in the lake drainage area, stabilizing the landscape and acting as traps and baffles to clastic sediments, thus reducing terrigenous input and minimizing their dilution effects on the OM.

Conversely, the deposition of saline lacustrine oil shales occurred under dry and cold climatic conditions exacerbated by declining CO_2 levels. Evaporation rates exceeding precipitation may have led to lower lake levels by decreasing freshwater inputs. Increased salinity resulted in more pronounced stratification, with reduced mixing between surface and bottom waters, creating more anoxic conditions at the lake bottom. The cooler climate and high salinity due to climate drought suppressed the productivity of algae and plankton, reducing the supply of aquatic

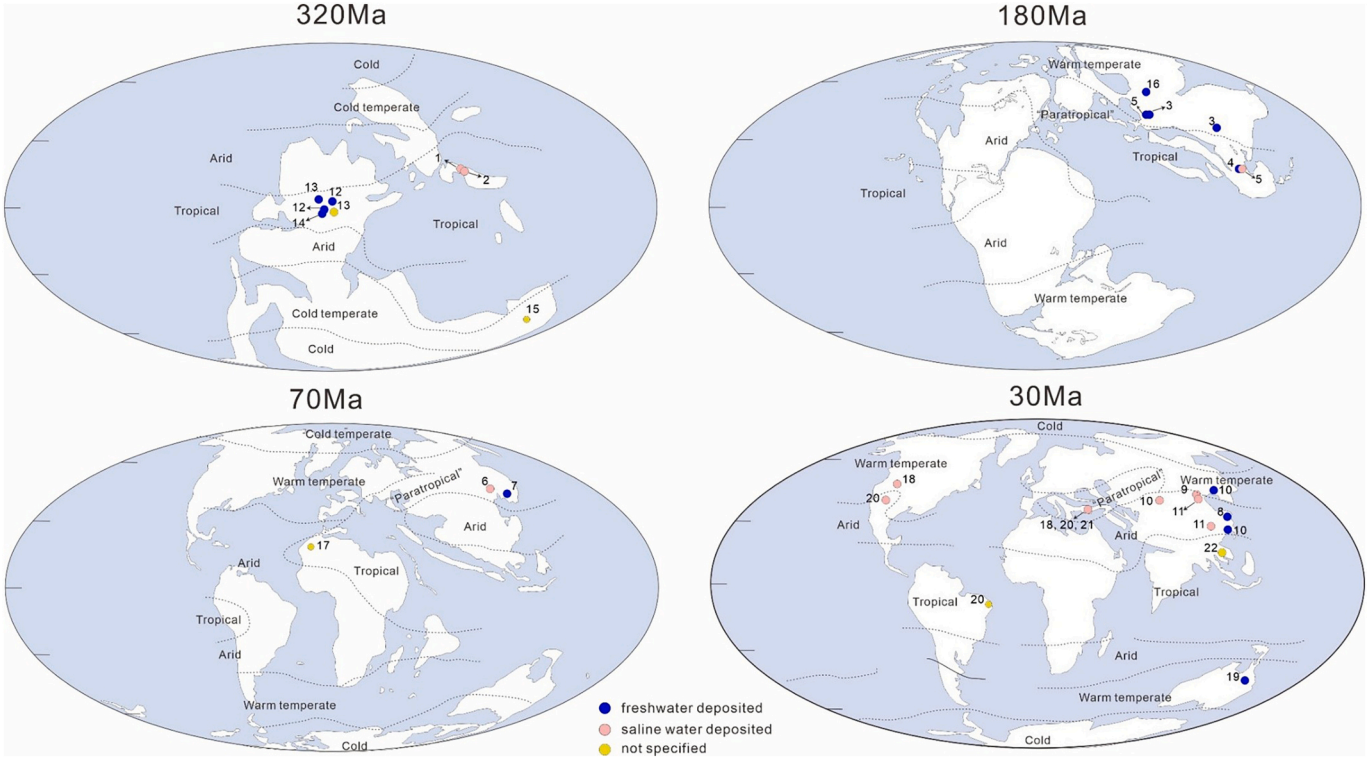

Fig. 8. Paleogeographic distribution of major lacustrine oil shales worldwide. Plate reconstructions are based on Scotese (2016) with paleoclimatic zones adapted from Boucot et al. (2013). Numbers on the map represent the major lacustrine oil shales in China and other regions of the world summarized in Table 1. Blue dots represent freshwater lacustrine oil shales, pink dots represent saline lacustrine oil shales, and yellow-green dots represent lacustrine oil shale of which the type of basin is unspecified. (For interpretation of the references to colour in this figure legend, the reader is referred to the web version of this article.)

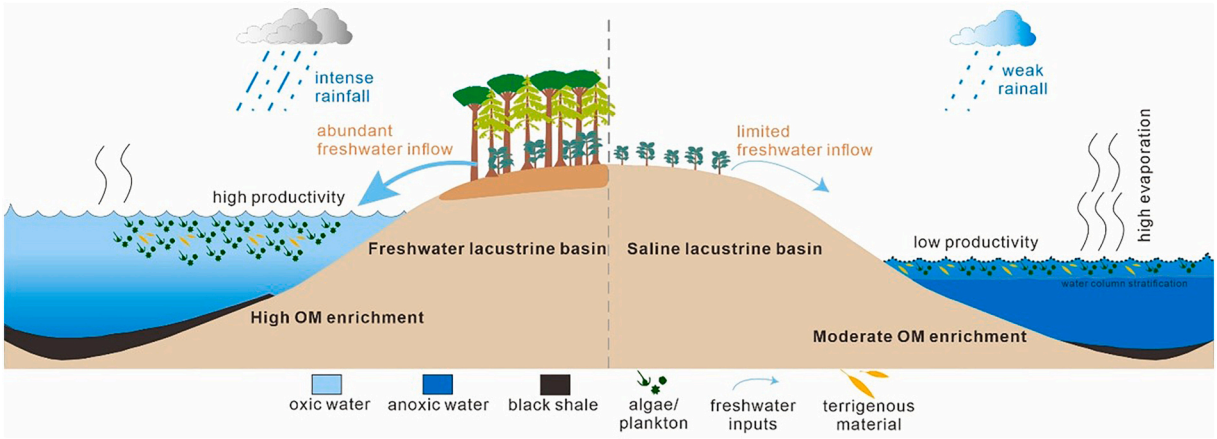

Fig. 9. Conceptual figure illustrating differential organic matter (OM) enrichment mechanisms influenced by paleoclimatic variations in freshwater and saline lacustrine basins.

OM. As lake levels dropped, the basins accommodated more terrigenous inputs, making the supply of terrigenous OM more significant. However, the increased detrital inputs diluted the OM in sediments, resulting in lower TOC content.

It is important to emphasize that the primary objective of this study is to assess the influence of paleoclimate on the differential OM enrichment between freshwater and saline water lacustrine oil shales. We recognize that other potential factors can also contribute to the formation of paleolakes of various salinity, leading to distinct OM enrichment characteristics. For example, tectonic activity exerts an influence, comparable to that of climate, on lacustrine deposits by regulating the balance of accommodation rates and influxes of sediments and water. This process can alter occurrence, distribution, and characteristics of lakes, ultimately shaping the depositional environments and influencing OM enrichment in lacustrine basins (Carroll and Bohacs, 1999; Pietras et al., 2003; Hao et al., 2011). However, due to the lack of quantitative indicators for regional-scale tectonic activity, this study could not apply machine learning methods to assess the influence of tectonic activity on the differential OM enrichment in freshwater and saline lacustrine basins.

In addition to paleoclimate variations and tectonic activity, other geological events, such as volcanic eruptions, hydrothermal activity, and gravity currents, also play a significant role in OM enrichment and are closely related to oil shale formation. For instance, volcanic gases or

ash can generate sulfate aerosols, which in turn influence the aerosol-cloud-climate feedback system, causing regional climatic changes that affect the depositional environment of lacustrine basins (Lohmann and Feichter, 2005; O'Dowd et al., 2004; Li et al., 2023). Volcanic and hydrothermal products are also rich in nutrients, which can lead to short-term algal blooms, enhancing OM accumulation (Langmann et al., 2010; Jones and Gislason, 2008; Hackley et al., 2017). Evidence of volcanic deposits and hydrothermal activity has been identified in saline lacustrine oil shales, such as the Permian Lucaogou Formation (Ding et al., 2023; Liu et al., 2013, 2015), as well as in freshwater lacustrine oil shales, such as the Yanchang Formation (Zhang et al., 2020) and the Qingshankou Formation (Peng et al., 2017; Liu et al., 2017a). While volcanic and hydrothermal activities undoubtedly contribute to OM enrichment, they may not be the primary factors responsible for the distinct developments of freshwater and saline lacustrine basins.

Besides the factors mentioned above, sedimentation rate is believed to play an important role in organic matter enrichment (Ibach, 1982; Tyson, 2001; Ahmat et al., 2016). Most previous studies have focused on the relationship between sedimentation rate and TOC in marine strata (e.g., Müller and Suess, 1979; Schulte et al., 2000). Ding et al. (2015) examined the relationship between sedimentation rate and TOC contents in eight lacustrine sections from the Erlian Basin in northern China. They suggested that when sedimentation rate is less than 5 cm/kyr, TOC content increases with sedimentation rate, whereas when sedimentation rate exceeds 5 cm/kyr, TOC content decreases with sedimentation rate. To assess the potential influence of sedimentation rate on the differential OM enrichment patterns of the freshwater and saline water lacustrine oil shales, we calculated the sedimentation rate of 7 studied lacustrine oil shales (see Supplementary Material for more details). Our results show the Shahejie and Kongdian formations have higher sedimentation rates than the other studied oil shales (Supplementary Fig. S2). No significant difference in sedimentation rates was found between the three saline lacustrine oil shales and the freshwater lacustrine oil shales (Supplementary Fig. S2). Therefore, we propose that sedimentation rate is not the primary factor for the higher TOC content in the freshwater lacustrine oil shales compared to the saline water lacustrine oil shales in China.

4. Conclusions and future work

This study is the first to apply a machine learning method to investigate the influence of paleoclimatic changes on OM enrichment mechanisms in the lacustrine oil shales in China. Using a RF classifier, we developed a new approach to discriminate between freshwater and saline lacustrine oil shales based on their bulk geochemical and molecular biomarker compositions of seven representative lacustrine oil shales in China. The results of classification presented above demonstrate a high performance of the RF technique for classifications of oil shales from variable environments. TOC content emerged as the most important factor for classification, with freshwater oil shales having higher TOC contents than saline counterparts.

Our MDA results indicate that such differential enrichment of OM in these two settings was influenced by a combination of factors, including paleoproductivity, paleowater conditions and terrigenous inputs, all driven by paleoclimate changes. However, the impact of each factor varied between the two settings. Freshwater lacustrine oil shales were generally deposited during warm and humid greenhouse periods, characterized by rising atmospheric CO_2 levels and greater precipitation, which promoted higher paleoproductivity and aquatic OM production. These conditions also reduced soil erosion by promoting the terrigenous plant growth, limiting the influx of terrigenous materials, and further enhancing OM enrichment. In contrast, saline lacustrine oil shales were predominantly deposited in the dry and cold icehouse periods, when elevated water salinity limited algal productivity, resulting in lower OM contents. Climatically driven differences in aqueous environments also had a pronounced impact on OM enrichment. In freshwater basins, humid climates reduced salinity and weakened water stratification, creating less reducing conditions. The bottom water environments were conducive to OM preservation as lake levels rose and terrestrial inputs declined. Conversely, in saline settings, high evaporation rates and low rainfall increased salinity and water stratification, creating more reducing environments.

This study highlights the critical role of paleoclimate in controlling OM enrichment and preservation in lacustrine settings. Our findings offer valuable insights into the formation and exploration potential of organic-rich lacustrine oil shales. However, we also acknowledge certain limitations in our study. Lacustrine depositional environments varied temporally and spatially, which could lead to differences in OM enrichment characteristics within the same type of lacustrine oil shales. For example, although both the Fengcheng and Lucaogou formations are Permian saline lake deposited oil shales in the Junggar Basin, the Fengcheng Formation yields an average TOC content of 1.1 wt%, which is significantly lower than the 4.3 wt% in the Lucaogou Formation. However, due to limitations in sample availability, this study did not conduct separate machine learning analyses on the organic geochemistry of each formation. Future work could expand on these results by incorporating additional geochemical data and refining the classifier to identify further categories of oil shales. Moreover, the statistical methods used here could be extended to other hydrocarbon resources to enhance exploration strategies.

Declaration of competing interest

The authors declare no competing interests.

Acknowledgements

This work was supported by National Natural Science Foundation of China (No. 42402137 and 42122016), and Science Foundation of China University of Petroleum, Beijing (No. 2462024BJRC006). We thank Jincai Duan, Yaxin Cui, Rui Zhao and Wenxin Hu for assistance with data collection. We thank Dr. Asfawossen Asrat, Dr. Simon George and two anonymous reviewers for detailed and thoughtful reviews.

Appendix A. Supplementary data

Supplementary data to this article can be found online at https://doi.org/10.1016/j.earscirev.2025.105061.

Data availability

Data shared as supplementary datasets

References

Abreu, S.F., 1949. Brazilian oil fields and oil-shale reserves. AAPG Bull. 33 (9), 1590–1599. https://doi.org/10.1306/3D933DF4-16B1-11D7-8645000102C1865D.

Ahmat, A.M., Boussafir, M., Milbeau, C.L., Guégan, R., Valdès, J., Guiñez, M., Sifeddine, A., Forestier, L.L., 2016. Organic matter-clay interaction along a seawater column of the Eastern Pacific upwelling system (Antofagasta bay, Chile): implications for source rock organic matter preservation. Mar. Chem. 179, 23–33. https://doi.org/10.1016/j.marchem.2016.01.003.

Algeo, T.J., Ingall, E., 2007. Sedimentary C_{org}:P ratios, paleocean ventilation, and Phanerozoic atmospheric pO_2. Palaeogeogr. Palaeoclimatol. Palaeoecol. 256 (3–4), 130–155. https://doi.org/10.1016/j.palaeo.2007.02.029.

Algeo, T.J., Maynard, J.B., 2004. Trace-element behavior and redox facies in core shales of Upper Pennsylvanian Kansas-type cyclothems. Chem. Geol. 206 (3–4), 289–318. https://doi.org/10.1016/j.chemgeo.2003.12.009.

Algeo, T.J., Tribovillard, N., 2009. Environmental analysis of paleoceanographic systems based on molybdenum–uranium covariation. Chem. Geol. 268 (3–4), 211–225. https://doi.org/10.1016/j.chemgeo.2009.09.001.

Altun, N.E., Hicyilmaz, C., Hwang, J.Y., Suat BaĞci, A., Kök, M., 2006. Oil Shales in the world and Turkey; reserves, current situation and future prospects: a review. Oil Shale 23 (3), 211–227. https://doi.org/10.3176/oil.2006.3.02.

Anderson, R.Y., Dean, W.E., 1988. Lacustrine varve formation through time. Palaeogeogr. Palaeoclimatol. Palaeoecol. 62 (1–4), 215–235. https://doi.org/10.1016/0031-0182(88)90055-7.

Ando, H., Hasegawa, H., Hasegawa, T., Ohta, T., Yamamoto, M., Hasebe, N., Li, G., Ichinnorov, N., 2011. Jurassic-cretaceous lacustrine deposits in the East Gobi Basin, Southeast Mongolia. J. Geol. Soc. Jpn. 117 (11). https://doi.org/10.5575/geosoc.117.11.XI_XIII. XI–XII.

Anguita, D., Ghelardoni, L., Ghio, A., Oneto, L., Ridella, S., 2012. The 'K' in K-fold cross validation. In: 20th European Symposium on Artificial Neural Networks, Computational Intelligence and Machine Learning (ESANN), pp. 441–446.

Avid, B., Purevsuren, B., 2001. Chemical composition of organic matter of the Mongolian Khoot oil shale. Oil Shale 18 (1), 15–23. https://doi.org/10.3176/oil.2001.1.03.

Bai, Y.L., Ma, Y.H., 2020. Geology of the Chang 7 Member oil shale of the Yanchang Formation of the Ordos Basin in central North China. Pet. Geosci. 26 (2), 355–371. https://doi.org/10.1144/petgeo2018-091.

Barry, R.G., Chorley, R.J., 2009. Atmosphere, Weather and Climate. Routledge, London. https://doi.org/10.4324/9780203871027.

Bejugam, P., Nayak, G.N., 2019. Tracing source–sink processes and productivity from trace metals (Ba, Zn, Pb, Cd) of the surface sediments off Mahanadi to Pennar, western Bay of Bengal. Environ. Earth Sci. 78, 1–11. https://doi.org/10.1007/s12665-019-8070-1.

Bell, W.A., 1958. Possibilities for Occurrence of Petroleum Reservoirs in Nova Scotia. Province of Nova Scotia, Department of Mines, Halifax, NS, p. 175.

Birgenheier, L.P., VandenBerg, M.D., Plink-Björklund, P., Gall, R.D., Rosencrans, E., Rosenberg, M.J., Toms, L.C., Morris, J., 2019. Climate impact on fluvial-lake system evolution, Eocene Green River Formation, Uinta Basin, Utah, USA. GSA Bull. 132, 562–587. https://doi.org/10.1130/B31808.1.

Boucot, A.J., Xu, C., Scotese, C.R., Morley, R.J., 2013. Phanerozoic paleoclimate: An atlas of lithologic indicators of climate. SEPM Concepts Sedimentol. Paleontol. 11, 1–478.

Bourbonniere, R.A., Meyers, P.A., 1996. Sedimentary geolipid records of historical changes in the watersheds and productivities of Lakes Ontario and Erie. Limnol. Oceanogr. 41 (2), 352–359. https://doi.org/10.4319/lo.1996.41.2.0352.

Brown, G.F., 1951. Geologic Reconnaissance of the Mineral Deposits of Thailand. US Government Printing Office.

Calvert, S.E., Pedersen, T.F., 2007. Elemental proxies for palaeoclimatic and palaeoceanographic variability in marine sediments: Interpretation and application. In: Hillaire-Marcel, C., De Vernal, A. (Eds.), Proxies in Late Cenozoic Paleoceanography Developments in Marine Geology 1. Elsevier, pp. 567–644. https://doi.org/10.1016/S1572-5480(07)01019-6.

Cao, J., Xia, L.W., Wang, T.T., Zhi, D.M., Tang, Y., Li, W.W., 2020. An alkaline lake in the late Paleozoic Ice Age (LPIA): a review and new insights into paleoenvironment and petroleum geology. Earth Sci. Rev. 202, 103091. https://doi.org/10.1016/j.earscirev.2020.103091.

Caplan, M.L., Bustin, R.M., 1999. Palaeoceanographic controls on geochemical characteristics of organic-rich Exshaw mudrocks: role of enhanced primary production. Org. Geochem. 30 (2–3), 161–188. https://doi.org/10.1016/S0146-6380(98)00202-2.

Carroll, A.R., Bohacs, K.M., 1999. Stratigraphic classification of ancient lakes: balancing tectonic and climatic controls. Geology 27 (2), 99–102. https://doi.org/10.1130/0091-7613(1999)027<0099:scoalb>2.3.co;2.

Castañeda, I.S., Schouten, S., 2011. A review of molecular organic proxies for examining modern and ancient lacustrine environments. Quat. Sci. Rev. 30 (21−22), 2851–2891. https://doi.org/10.1016/j.quascirev.2011.07.009.

Chamberlain, C.P., Wan, X.Q., Graham, S.A., Carroll, A.R., Doebbert, A.C., Sageman, B. B., Blisniuk, P., Kent-Corson, M.L., Wang, Z., Wang, C.S., 2013. Stable isotopic evidence for climate and basin evolution of the late cretaceous Songliao Basin, China. Palaeogeogr. Palaeoclimatol. Palaeoecol. 385, 106–124. https://doi.org/10.1016/j.palaeo.2012.03.020.

Chen, J., An, Z.S., Head, J., 1999. Variation of Rb/Sr ratios in the loess-paleosol sequences of Central China during the last 130,000 years and their implications for monsoon paleoclimatology. Quat. Res. 51 (3), 215–219. https://doi.org/10.1006/qres.1999.2038.

Chen, J., Wang, Y.J., Chen, Y., Liu, L.W., Ji, J.F., Lu, H.Y., 2001. Rb and Sr geochemical characterization of the Chinese loess and its implications for palaeomonsoon climate. Acta Geol. Sin. 75 (2), 259–266.

Chen, Y.H., Zhu, Z.W., Zhang, L., 2019. Control actions of sedimentary environments and sedimentation rates on lacustrine oil shale distribution, an example of the oil shale in the Upper Triassic Yanchang Formation, southeastern Ordos Basin (NW China). Mar. Pet. Geol. 102, 508–520. https://doi.org/10.1016/j.marpetgeo.2019.01.006.

Chen, Z.L., Ding, Z.L., Tang, Z.H., Yang, S.L., Wang, X., Cui, L.L., 2017. Paleoweathering and paleoenvironmental change recorded in lacustrine sediments of the early to middle Eocene in Fushun Basin, Northeast China. Geochem. Geophys. Geosyst. 18 (1), 41–51. https://doi.org/10.1002/2016GC006573.

Cheng, P., Gai, H.F., Xiao, X.M., Zhou, L.Y., Zhao, W., Zhou, Q., Tian, H., 2023. Evolution of the pristane/phytane ratio with maturity of lacustrine source rocks: Implications of a thermal simulation experiment. ACS Earth Space Chem. 7 (5), 1072–1082. https://doi.org/10.1021/acsearthspacechem.3c00011.

Cranwell, P.A., Eglinton, G., Robinson, N., 1987. Lipids of aquatic organisms as potential contributors to lacustrine sediments—II. Org. Geochem. 11 (6), 513–527. https://doi.org/10.1016/0146-6380(87)90007-6.

Cui, D.Y., Liang, S.L., Wang, D.D., 2021. Observed and projected changes in global climate zones based on Köppen climate classification. Wiley Interdiscip. Rev. Clim. Chang. 12 (3), 1–28. https://doi.org/10.1002/wcc.701.

Curiale, J.A., Gibling, M.R., 1994. Productivity control on oil shale formation—Mae Sot Basin, Thailand. Org. Geochem. 21 (1), 67–89. https://doi.org/10.1016/0146-6380(94)90088-4.

Davies, G., Nassichuk, W., 1988. An early Carboniferous (Viséan) lacustrine oil shale in Canadian Arctic Archipelago. AAPG Bull. 72 (1), 8–20. https://doi.org/10.1306/703C81B9-1707-11D7-8645000102C1865D.

Deng, T., Li, Y., Wang, Z.J., Yu, Q., Dong, S.L., Yan, L., Hu, W.C., Chen, B., 2019. Geochemical characteristics and organic matter enrichment mechanism of black shale in the Upper Triassic Xujiahe Formation in the Sichuan Basin: implications for paleoweathering, provenance and tectonic setting. Mar. Pet. Geol. 109, 698–716. https://doi.org/10.1016/j.marpetgeo.2019.06.057.

Didyk, B.M., Simoneit, B.R.T., Brassell, S.C., Eglinton, G., 1978. Organic geochemical indicators of palaeoenvironmental conditions of sedimentation. Nature 272 (5650), 216–222. https://doi.org/10.1038/272216a0.

Ding, W.J., Hou, D.J., Li, L., Jiang, L., Zhang, Z.M., Jiang, Y.H., George, S.C., 2024. Reconstructing the palaeoecology of a Middle Permian alkaline lake using molecular fossils, case study of the Lucaogou Formation in the Junggar Basin, NW China. Org. Geochem. 193, 104791. https://doi.org/10.1016/j.orggeochem.2024.104791.

Ding, X.J., Liu, G.D., Zha, M., Huang, Z.L., Gao, C.H., Lu, X.J., Sun, M.L., Chen, Z.L., Liuzhuang, X.X., 2015. Relationship between total organic carbon content and sedimentation rate in ancient lacustrine sediments, a case study of Erlian Basin, northern China. J. Geochem. Explor. 149, 22–29. https://doi.org/10.1016/j.gexplo.2014.11.004.

Ding, X.J., Qu, J.X., Imin, A., Zha, M., Su, Y., Jiang, Z.F., Jiang, H., 2019. Organic matter origin and accumulation in tuffaceous shale of the lower Permian Lucaogou Formation, Jimsar Sag. J. Pet. Sci. Eng. 179, 696–706. https://doi.org/10.1016/j.petrol.2019.05.004.

Ding, X.J., Qian, L.R., Jiang, W.L., Yiming, A., Cao, Z., Jiang, Z.F., Zha, M., 2023. Volcanic ash content of Permian Lucagou shale in the Jimsar sag, Junggar Basin: evidence from comprehensive analysis of mercury (Hg), major elements, strontium isotope, and thin section. Mar. Pet. Geol. 157, 106501. https://doi.org/10.1016/j.marpetgeo.2023.106501.

Dixon, D.A., Pope, G.J., 1987. Oil shale of the Duaringa Basin, Central Queensland. Fuel 66 (3), 305–308. https://doi.org/10.1016/0016-2361(87)90083-4.

Duan, H., Liu, S., Fu, Q., 2020. Characteristics and sedimentary environment of organic-rich shale in the second member of Paleogene Funing Formation, Subei Basin. Petrol. Geol. Exper. 42 (4), 612–617. https://doi.org/10.11781/sysydz202004612.

Dutta, S., Greenwood, P.F., Brocke, R., Schaefer, R.G., Mann, U., 2006. New insights into the relationship between *Tasmanites* and tricyclic terpenoids. Org. Geochem. 37 (1), 117–127. https://doi.org/10.1016/j.orggeem.2005.08.010.

Dyni, J.R., 2003. Geology and Resources of Some World Oil-Shale Deposits: U.S. Geological Survey Scientific Investigations Report 2005–5294, 42 pp. https://doi.org/10.3176/oil.2003.3.02.

Eglinton, G., Hamilton, R.J., 1967. Leaf epicuticular waxes: the waxy outer surfaces of most plants display a wide diversity of fine structure and chemical constituents. Science 156 (3780), 1322–1335. https://doi.org/10.1126/science.156.3780.1322.

Embry, A.F., Beauchamp, B., 2008. Sverdrup Basin, Chapter 13. In: Miall, A.D. (Ed.), Sedimentary Basins of the World. The Sedimentary Basins of the United States and Canada, vol. 5. Elsevier, Amsterdam, Netherlands, pp. 451–471.

Endo, S., 1966. Some late Mesozoic and late Tertiary plants and a fossil insect from Thailand. Jap. J. Geol. Geogr. 37 (2–4), 191–193.

Erdenetsogt, B.O., Hong, S.K., Choi, J., Lee, I., 2022. Depositional environment and petroleum source rock potential of Mesozoic lacustrine sedimentary rocks in Central Mongolia. Mar. Pet. Geol. 140, 105646. https://doi.org/10.1016/j.marpetgeo.2022.105646.

Fan, P., Philp, R.P., Li, Z.X., Yu, X.K., Ying, G.G., 1991. Biomarker distributions in crude oils and source rocks from different sedimentary environments. Chem. Geol. 93 (1–2), 61–78. https://doi.org/10.1016/0009-2541(91)90064-X.

Fang, Z., Chen, S.Y., Pu, X.G., Yan, J.H., Chen, X.R., 2022. Control of sedimentary environment on the lithofacies of lacustrine fine-grained sedimentary rocks in the second member of the Kongdian Formation in the Cangdong Sag, Bohai Bay Basin, China. Geol. J. 57 (6), 2321–2345. https://doi.org/10.1002/gj.4413.

Ficken, K.J., Li, B., Swain, D.L., Eglinton, G., 2000. An *n*-alkane proxy for the sedimentary input of submerged/floating freshwater aquatic macrophytes. Org. Geochem. 31 (7–8), 745–749. https://doi.org/10.1016/S0146-6380(00)00081-4.

Foster, G.L., Royer, D.L., Lunt, D.J., 2017. Future climate forcing potentially without precedent in the last 420 million years. Nat. Commun. 8 (1), 14845. https://doi.org/10.1038/ncomms14845.

Fu, J.M., Sheng, G.Y., An, P.P., Brassell, S.C., Eglinton, G., Gang, J.J., 1986. Peculiarities of salt lake sediments as potential source rocks in China. Org. Geochem. 10 (1–3), 119–126. https://doi.org/10.1016/0146-6380(86)90015-X.

Gallego-Torres, D., Martínez-Ruiz, F., Paytan, A., Jiménez-Espejo, F.J., Ortega-Huertas, M., 2007. Pliocene–Holocene evolution of depositional conditions in the eastern Mediterranean: role of anoxia vs. productivity at time of sapropel deposition. Palaeogeogr. Palaeoclimatol. Palaeoecol. 246 (2–4), 424–439. https://doi.org/10.1016/j.palaeo.2006.10.008.

Gao, G., Zhang, W.W., Xiang, B.L., Liu, G.D., Ren, J.L., 2016. Geochemistry characteristics and hydrocarbon-generating potential of lacustrine source rock in Lucaogou Formation of the Jimusaer Sag, Junggar Basin. J. Pet. Sci. Eng. 145, 168–182. https://doi.org/10.1016/j.petrol.2016.03.023.

Gao, G., Titi, A., Yang, S.R., Tang, Y., Kong, Y.H., He, W.J., 2017. Geochemistry and depositional environment of fresh lacustrine source rock: a case study from the Triassic Baijiantan Formation shales in Junggar Basin, Northwest China. Org. Geochem. 113, 75–89. https://doi.org/10.1016/j.orggeochem.2017.08.002.

Gehlen, M., Beck, L., Calas, G., Flank, A.M., Van Bennekom, A.J., Van Beusekom, J., 2002. Unraveling the atomic structure of biogenic silica: evidence of the structural association of Al and Si in diatom frustules. Geochim. Cosmochim. Acta 66 (9), 1601–1609. https://doi.org/10.1016/S0016-7037(01)00877-8.

Gibson, D., 1980. Oil shale in Australia: its occurrence and resources. Aust. Miner. Ind. 33 (3), 105–113.

Gibson, P., 1989. Petrology of two Tertiary oil shale deposits from Queensland, Australia. J. Geol. Soc. 146 (2), 319–331. https://doi.org/10.1144/gsjgs.146.2.0319.

Glikson-Simpson, M., 2021. Tertiary oil shales in Australia: Rundle complex. In: Oil Shales. Springer, Cham, pp. 79–99. https://doi.org/10.1007/978-3-030-60675-6_5.
Goldberg, K., Humayun, M., 2010. The applicability of the chemical index of Alteration as a paleoclimatic indicator: an example from the Permian of the Paraná Basin, Brazil. Palaeogeogr. Palaeoclimatol. Palaeoecol. 293 (1–2), 175–183. https://doi.org/10.1016/j.palaeo.2010.05.015.
Goodarzi, F., 2020a. A climate change event, detected in Viséan oil shales from Devon Island, Arctic Canada. Int. J. Coal Geol. 226, 103503. https://doi.org/10.1016/j.coal.2020.103503.
Goodarzi, F., 2020b. Comparison of the geochemistry of lacustrine oil shales of Mississippian age from Nova Scotia and New Brunswick, Canada. Int. J. Coal Geol. 220, 103398. https://doi.org/10.1016/j.coal.2020.103398.
Goodarzi, F., Gentzis, T., Sanei, H., Pedersen, P.K., 2019a. Elemental composition and organic petrology of a lower Carboniferous-age freshwater oil shale in Nova Scotia, Canada. ACS Omega 4 (24), 20773–20786. https://doi.org/10.1021/acsomega.9b03227.
Goodarzi, F., Haeri-Ardakani, O., Gentzis, T., Pedersen, P., 2019b. Organic petrology and geochemistry of Tournaisian-age Albert Formation oil shales, New Brunswick, Canada. Int. J. Coal Geol. 205, 43–57. https://doi.org/10.1016/j.coal.2019.01.015.
Goodarzi, F., Goodarzi, N., Malachowska, A., 2021. Elemental composition, environment of deposition of the lower Carboniferous Emma Fiord formation oil shale in Arctic Canada. Int. J. Coal Geol. 244, 103715. https://doi.org/10.1016/j.coal.2021.103715.
Green, P., Bateman, R., 1981. The geology of the Condor oil shale deposit—onshore Hillsborough Basin. APEA J. 21 (1), 24–32. https://doi.org/10.1071/AJ80003.
Guelbay, R., Korkmaz, S., 2008. Organic geochemistry, depositional environment and hydrocarbon potential of the Tertiary oil shale deposits in NW Anatolia, Turkey. Oil Shale 25 (4). https://doi.org/10.3176/oil.2008.4.05.
Guo, Z.X., Shi, Y.P., Yang, Y.T., Jiang, S.Q., Li, L.B., Zhao, Z.G., 2018. Inversion of the Erlian Basin (NE China) in the early late cretaceous: Implications for the collision of the Okhotomorsk Block with East Asia. J. Asian Earth Sci. 154, 49–66. https://doi.org/10.1016/j.jseaes.2017.12.007.
Hackley, P.C., Walters, C.C., Kelemen, S.R., Mastalerz, M., Lowers, H.A., 2017. Organic petrology and micro-spectroscopy of Tasmanites microfossils: applications to kerogen transformations in the early oil window. Org. Geochem. 114, 23–44. https://doi.org/10.1016/j.orggeochem.2017.09.002.
Hao, F., Zhou, X.H., Zhu, Y.M., Yang, Y.Y., 2011. Lacustrine source rock deposition in response to co-evolution of environments and organisms controlled by tectonic subsidence and climate, Bohai Bay Basin, China. Org. Geochem. 42 (4), 323–339. https://doi.org/10.1016/j.orggeochem.2011.01.010.
Hasegawa, H., Ando, H., Hasebe, N., Ichinnorov, N., Ohta, T., Hasegawa, T., Yamamoto, M., Li, G., Erdenetsogt, B.O., Heimhofer, U., 2018. Depositional ages and characteristics of Middle–Upper Jurassic and Lower Cretaceous lacustrine deposits in southeastern Mongolia. Island Arc 27 (3), e12243. https://doi.org/10.1111/iar.12243.
He, W.T., Sun, Y.H., Guo, W., Shan, X.L., Su, S.Y., Zheng, S.P., Deng, S.H., Kang, S.J., Zhang, X., 2019. Organic geochemical characteristics of the Upper cretaceous Qingshankou Formation oil shales in the Fuyu oilfield, Songliao Basin, China: implications for oil-generation potential and depositional environment. Energies 12 (24), 4778. https://doi.org/10.3390/en12244778.
Herman, A.B., Spicer, R.A., Aleksandrova, G.N., Yang, J., Kodrul, T.M., Maslova, N.P., Spicer, T.E., Chen, G., Jin, J.H., 2017. Eocene–Early Oligocene climate and vegetation change in southern China: evidence from the Maoming Basin. Palaeogeogr. Palaeoclimatol. Palaeoecol. 479, 126–137. https://doi.org/10.1016/j.palaeo.2017.04.023.
Herzsprung, P., Wentzky, V., Kamjunke, N., von Tümpling, W., Wilske, C., Friese, K., Boehrer, B., Reemtsma, T., Rinke, K., Lechtenfeld, O.J., 2020. Improved understanding of dissolved organic matter processing in freshwater using complementary experimental and machine learning approaches. Environ. Sci. Technol. 54 (21), 13556–13565. https://doi.org/10.1021/acs.est.0c02383.
Hofer, G., Wagreich, M., Neuhuber, S., 2013. Geochemistry of fine-grained sediments of the Upper cretaceous to Paleogene Gosau Group (Austria, Slovakia): implications for paleoenvironmental and provenance studies. Geosci. Front. 4 (4), 449–468. https://doi.org/10.1016/j.gsf.2012.11.009.
Hoggard, M.J., Czarnota, K., Richards, F.D., Huston, D.L., Jaques, A.L., Ghelichkhan, S., 2020. Global distribution of sediment-hosted metals controlled by craton edge stability. Nat. Geosci. 13 (7), 504–510.
Hong, Y.C., Yang, Z.Q., Wang, S.T., Sun, X.J., Du, N.Q., Sun, M.R., Li, Y.G., 1980. A Research on the Strata and Palaeontology of the Fushun Coal Field in Liaoning Province (in Chinese with English Abstract). Science Press, Beijing.
Horsfield, B., Curry, D.J., Bohacs, K., Littke, R., Rullkötter, J., Schenk, H.J., Radke, M., Schaefer, R.G., Carroll, A.R., Isaksen, G., 1994. Organic geochemistry of freshwater and alkaline lacustrine sediments in the Green River Formation of the Washakie Basin, Wyoming, USA. Org. Geochem. 22 (3–5), 415–440. https://doi.org/10.1016/0146-6380(94)90117-1.
Hou, D.J., Li, M.W., Huang, Q.H., 2000. Marine transgressional events in the gigantic freshwater lake Songliao: Paleontological and geochemical evidence. Org. Geochem. 31 (7–8), 763–768. https://doi.org/10.1016/S0146-6380(00)00065-6.
Huang, D.Y., 2019. Jurassic integrative stratigraphy and timescale of China. Sci. China Earth Sci. 62, 223–255. https://doi.org/10.1007/s11430-017-9268-7.
Huang, Y.J., Yang, G.S., Gu, J., Wang, P.K., Huang, Q.H., Feng, Z.H., Feng, L.J., 2013. Marine incursion events in the late cretaceous Songliao Basin: constraints from sulfur geochemistry records. Palaeogeogr. Palaeoclimatol. Palaeoecol. 385, 152–161. https://doi.org/10.1016/j.palaeo.2013.03.017.
Hughes, W.B., Holba, A.G., Dzou, L.I., 1995. The ratios of dibenzothiophene to phenanthrene and pristane to phytane as indicators of depositional environment and lithology of petroleum source rocks. Geochim. Cosmochim. Acta 59 (17), 3581–3598. https://doi.org/10.1016/0016-7037(95)00225-O.
Hupp, B.N., Weislogel, A.L., 2018. Geochemical insights into provenance of the Middle Devonian Hamilton group of the central Appalachian Basin, USA. J. Sediment. Res. 88 (10), 1153–1165. https://doi.org/10.2110/jsr.2018.62.
Hutton, A., 1988. The lacustrine Condor oil shale sequence. Geo. Soc. London, Spec. Publ. 40 (1), 329–340. https://doi.org/10.1144/GSL.SP.1988.040.01.27.
Hyde, R.S., 1984. Geological history of the Carboniferous deer Lake Basin, west-central Newfoundland, Canada. In: Geltzer, H.H.J., Nassichuk, W.W., Belt, E.S., Mcqueen, R. W. (Eds.), Atlantic Coast Basins, Paleogeography and Paleotectonics, Sedimentology and Geochemistry. Ninth International Congress of Carboniferous Stratigraphy and Geology. Carbondale, Illinois, Vol. 3, pp. 85–104.
Ibach, L.E.J., 1982. Relationship between sedimentation rate and total organic carbon content in ancient marine sediments. AAPG Bull. 66, 170–188.
Jia, C.Z., Zheng, M., Zhang, Y.F., 2012. Unconventional hydrocarbon resources in China and the prospect of exploration and development. Pet. Explor. Dev. 39 (2), 139–146. https://doi.org/10.1016/S1876-3804(12)60026-3.
Jia, J.L., Bechtel, A., Liu, Z.J., Strobl, S.A., Sun, P.C., Sachsenhofer, R.F., 2013a. Oil shale formation in the Upper cretaceous Nenjiang Formation of the Songliao Basin (NE China): implications from organic and inorganic geochemical analyses. Int. J. Coal Geol. 113, 11–26. https://doi.org/10.1016/j.coal.2013.03.004.
Jia, J.L., Liu, Z.J., Bechtel, A., Strobl, S.A., Sun, P.C., 2013b. Tectonic and climate control of oil shale deposition in the Upper cretaceous Qingshankou Formation (Songliao Basin, NE China). Int. J. Earth Sci. 102, 1717–1734. https://doi.org/10.1007/s00531-013-0903-7.
Jin, Q., Zhu, G.Y., 2006. Progress in research of deposition of oil source rocks in saline lake and their hydrocarbon generation. Geol. J. China Univ. 12 (4), 483–492.
Jin, Z.J., Wang, X.M., Wang, H.J., Ye, Y.T., Zhang, S.C., 2023. Organic carbon cycling and black shale deposition: an Earth System Science perspective. Natl. Sci. Rev. 10 (11), nwad243. https://doi.org/10.1093/nsr/nwad243.
Johnson, R.C., Birdwell, J.E., Dolan, M.P., Higley, D.H., Lillis, P.G., 2016. Evolution of the lower Tertiary Elko lake basin, a potential hydrocarbon source rock in Northeast Nevada. In: Dolan, M.P., Higley, D.H., Lillis, P.G. (Eds.), Hydrocarbon Source Rocks in Unconventional Plays, Rocky Mountain Region. Rocky Mountain Association of Geologists, pp. 261–294.
Jones, M.T., Gislason, S.R., 2008. Rapid releases of metal salts and nutrients following the deposition of volcanic ash into aqueous environments. Geochim. Cosmochim. Acta 72 (15), 3661–3680. https://doi.org/10.1016/j.gca.2008.05.030.
Katz, B.J., 2005. Controlling factors on source rock development—A review of productivity, preservation and sedimentation rate. In: Harris, N.B. (Ed.), The Deposition of Organic-Carbon-Rich Sediments: Models, Mechanisms, and Consequences: Tulsa, vol. 82. SEPM Special Publication, Oklahoma, pp. 7–16. https://doi.org/10.2110/pec.05.82.0007.
Knaus, E., Killen, J., Biglarbigi, K., Crawford, P., 2010. An overview of oil shale resources. In: Ogunsola, O.I., Hartstein, A.M., Ogunsola, O. (Eds.), Oil Shale: A Solution to the Liquid Fuel Dilemma, vol. 1032. American Chemical Society, pp. 3–20. https://doi.org/10.1021/bk-2010-1032.ch001.
Kodner, R.B., Pearson, A., Summons, R.E., Knoll, A.H., 2008. Sterols in red and green algae: quantification, phylogeny, and relevance for the interpretation of geologic steranes. Geobiol 6 (4), 411–420. https://doi.org/10.1111/j.1472-4669.2008.00167.x.
Kribii, A., Lemée, L., Chaouch, A., Amblès, A., 2001. Structural study of the Moroccan Timahdit (Y-layer) oil shale kerogen using chemical degradations. Fuel 80 (5), 681–691. https://doi.org/10.1016/s0140-6701(02)85084-6.
Langmann, B., Zakšek, K., Hort, M., Duggen, S., 2010. Volcanic ash as fertiliser for the surface ocean. Atmos. Chem. Phys. 10 (8), 3891–3899. https://doi.org/10.5194/acp-10-3891-2010.
Lary, D.J., Alavi, A.H., Gandomi, A.H., Walker, A.L., 2016. Machine learning in geosciences and remote sensing. Geosci. Front. 7 (1), 3–10. https://doi.org/10.1016/j.gsf.2015.07.003.
Lash, G.G., Blood, D.R., 2014. Organic matter accumulation, redox, and diagenetic history of the Marcellus Formation, southwestern Pennsylvania, Appalachian Basin. Mar. Pet. Geol. 57, 244–263. https://doi.org/10.1016/j.marpetgeo.2014.06.001.
Lee, C., 1992. Controls on organic carbon preservation: the use of stratified water bodies to compare intrinsic rates of decomposition in oxic and anoxic systems. Geochim. Cosmochim. Acta 56 (8), 3323–3335. https://doi.org/10.1016/0016-7037(92)90308-6.
Lerman, A., Imboden, D.M., Gat, J.R., Chou, L., 1995. Physics and Chemistry of Lakes. Springer-Verlag, Berlin.
Li, D.L., Li, R.X., Zhu, Z.W., Wu, X.L., Cheng, J.H., Liu, F.T., Zhao, B.S., 2017. Origin of organic matter and paleo-sedimentary environment reconstruction of the Triassic oil shale in Tongchuan City, southern Ordos Basin (China). Fuel 208, 223–235. https://doi.org/10.1016/j.fuel.2017.07.008.
Li, D.L., Wu, S.Q., He, Q.Y., Li, W.P., Meng, P.L., Li, H.B., Sun, Q., Zhao, X.C., 2024a. Comprehensive comparison of lacustrine fine-grained sedimentary rock reservoirs, organic matter, and palaeoenvironment: a case study of the Jurassic Ziliujing Formation and Xintiangou Formation in the Sichuan Basin. Minerals 14 (4), 336. https://doi.org/10.3390/min14040336.
Li, G., Ando, H., Hasegawa, H., Yamamoto, M., Hasegawa, T., Ohta, T., Hasebe, N., Ichinnorov, N., 2014. Confirmation of a Middle Jurassic age for the Eedemt Formation in Dundgobi Province, Southeast Mongolia: constraints from the discovery of new spinicaudatans (clam shrimps). Alcheringa 38 (3), 305–316. https://doi.org/10.1080/03115518.2014.870834.
Li, J.H., Fang, Y.N., Jarzembowski, E.A., Li, T., Teng, X., Zhang, Q.Q., Peng, J.G., Sha, J. G., 2024b. The Sangonghe biota in the Junggar Basin, NW China: age constraints and

climate implications. Hist. Biol. 36 (8), 1655–1662. https://doi.org/10.1080/08912963.2023.2223215.
Li, L., Liu, Z.J., Jiang, L., George, S.C., 2021. Organic petrology and geochemistry of lower cretaceous lacustrine sediments in the Chaoyang Basin (Liaoning Province, Northeast China): influence of volcanic ash on algal productivity and oil shale formation. Int. J. Coal Geol. 233, 103653. https://doi.org/10.1016/j.coal.2020.103653.
Li, L., He, W.T., Liu, Z.J., Song, Y., Li, Y.J., Belousova, E., Löhr, S.C., George, S.C., 2023. Volcanic activity drives lacustrine carbon sequestration after Oceanic Anoxic Event 1a. Palaeogeogr. Palaeoclimatol. Palaeoecol. 621, 111595. https://doi.org/10.1016/j.palaeo.2023.111595.
Li, M.J., Wang, T.G., Zhong, N.N., Zhang, W.B., Sadik, A., Li, H.B., 2013. Ternary diagram of fluorenes, dibenzothiophenes and dibenzofurans: indicating depositional environment of crude oil source rocks. Energy Explor. Exploit. 31 (4), 569–588. https://doi.org/10.1260/0144-5987.31.4.569.
Li, M.W., Chen, Z.H., Cao, T.T., Ma, X.X., Liu, X.J., Li, Z.M., Jiang, Q.G., Wu, S.Q., 2018. Expelled oils and their impacts on rock-eval data interpretation, Eocene Qianjiang Formation in Jianghan Basin, China. Int. J. Coal Geol. 191, 37–48. https://doi.org/10.1016/j.coal.2018.03.001.
Li, M.W., Ma, X.X., Jin, Z.J., Li, Z.M., Jiang, Q.G., Wu, S.Q., Li, Z., Xu, Z.X., 2022a. Diversity in the lithofacies assemblages of marine and lacustrine shale strata and significance for unconventional petroleum exploration in China. Oil Gas Geol. 43 (1), 1–25. https://doi.org/10.11743/ogg20220101.
Li, P., Liu, Z.B., Bi, H., Jiang, T., Bian, R.K., Wang, P.W., Shang, X.Y., 2024c. Differences in and factors controlling organic matter enrichment in the Ziliujing Formation shale in the Sichuan Basin. Pet. Sci. 21 (1), 77–86. https://doi.org/10.1016/j.petsci.2023.10.020.
Li, X., Hu, Y.Y., Guo, J.Q., Lan, J.W., Lin, Q.F., Bao, X.J., Yuan, S., Wei, M.Y., Li, Z.B., Man, K., 2022b. A high-resolution climate simulation dataset for the past 540 million years. Sci. Data 9 (1), 371. https://doi.org/10.1038/s41597-022-01490-4.
Liu, B., Lü, Y.F., Meng, Y.L., Li, X.N., Guo, X.B., Ma, Q., Zhao, W.C., 2015. Petrologic characteristics and genetic model of lacustrine lamellar fine-grained rock and its significance for shale oil exploration: a case study of Permian Lucaogou Formation in Malang Sag, Santanghu Basin, NW China. Pet. Explor. Dev. 42 (5), 656–666. https://doi.org/10.1016/S1876-3804(15)30060-4.
Liu, C.L., Wang, Z.L., Guo, Z.Q., Hong, W.Y., Dun, C., Zhang, X., Li, B., Wu, L.Q., 2017a. Enrichment and distribution of shale oil in the cretaceous Qingshankou Formation, Songliao Basin, Northeast China. Mar. Pet. Geol. 86, 751–770. https://doi.org/10.1016/j.marpetgeo.2017.06.034.
Liu, Q.X., Song, Y., Jiang, L., Cao, T., Chen, Z.H., Xiao, D.Q., Han, G.M., Ji, W.M., Gao, F.L., Wang, P.T., 2017b. Geochemistry and correlation of oils and source rocks in Banqiao Sag, Huanghua Depression, northern China. Int. J. Coal Geol. 176, 49–68. https://doi.org/10.1016/j.coal.2017.04.005.
Liu, Q.Y., Li, P., Jin, Z.J., Sun, Y.W., Hu, G., Zhu, D.Y., Huang, Z.K., Liang, X.P., Zhang, R., Liu, J.Y., 2022. Organic-rich formation and hydrocarbon enrichment of lacustrine shale strata: a case study of Chang 7 Member. Sci. China Earth Sci. 65, 118–138. https://doi.org/10.1007/s11430-021-9819-y.
Liu, Q.Y., Li, P., Jiang, L., Jin, Z.J., Liang, X.P., Zhu, D.Y., Pang, Q., Zhang, R., Liu, J.Y., 2024. Distinctive volcanic ash–rich lacustrine shale deposition related to chemical weathering intensity during the late Triassic: evidence from lithium contents and isotopes. Sci. Adv. 10 (11), eadi6594. https://doi.org/10.1126/sciadv.adi6594.
Liu, Y.Q., Zhou, D.W., Jiao, X., Nan, Y., Yang, W., Li, H., Zhou, X.H., 2013. A new type of sedimentary rocks: Mantle-originated hydroclastites and hydrothermal exhalites, Santanghu area, Xinjiang, NW China. Acta Sedimentol. Sin. 31 (5), 773–781.
Liu, Z.J., Yang, H.L., Dong, Q.S., Zhu, J.W., Guo, W., Ye, S.Q., Liu, R., Meng, Q.T., Zhang, H.L., Gan, S.C., 2009. Oil Shale in China (in Chinese). Petroleum Industry Press, Beijing.
Lohmann, U., Feichter, J., 2005. Global indirect aerosol effects: a review. Atmos. Chem. Phys. 5 (3), 715–737. https://doi.org/10.5194/acp-5-715-2005.
Loureiro, M.R.B., Cardoso, J.N., 1990. Aromatic hydrocarbons in the Paraiba Valley oil shale. Org. Geochem. 15 (4), 351–359. https://doi.org/10.1016/0146-6380(90)90161-R.
Lu, M., Lu, Y.H., Ikejiri, T., Sun, D.Y., Carroll, R., Blair, E.H., Algeo, T.J., Sun, Y., 2021. Periodic oceanic euxinia and terrestrial fluxes linked to astronomical forcing during the Late Devonian Frasnian–Famennian mass extinction. Earth Planet. Sci. Lett. 562, 116839. https://doi.org/10.1016/j.epsl.2021.116839.
Lu, Y., Meyers, P.A., 2009. Sediment lipid biomarkers as recorders of the contamination and cultural eutrophication of Lake Erie, 1909–2003. Org. Geochem. 40 (8), 912–921.
Luo, Q.Y., Zhong, N.N., Liu, Y., Qu, Y.S., Ma, L., 2018. Organic geochemical characteristics and accumulation of the organic matter in the Jurassic to cretaceous sediments of the Saihantala Sag, Erlian Basin, China. Mar. Pet. Geol. 92, 855–867. https://doi.org/10.1016/j.marpetgeo.2018.01.002.
Luo, Q.Y., Fariborz, G., Zhong, N.N., Wang, Y., Qiu, N.S., Skovsted, C.B., Suchý, V., Schovsbo, N.H., Morga, R., Xu, Y.H., Hao, J.Y., Liu, A.J., Wu, J., Cao, W.X., Min, X., Wu, J., 2020. Graptolites as fossil geo-thermometers and source material of hydrocarbons: an overview of four decades of progress. Earth Sci. Rev. 200, 103000. https://doi.org/10.1016/j.earscirev.2019.103000.
Lv, D.W., Wang, L.J., Isbell, J.L., Lu, C.Y., Li, P.P., Wang, Y.J., Zhang, Z.H., 2022. Records of chemical weathering and volcanism linked to paleoclimate transition during the late Paleozoic Icehouse. Glob. Planet. Chang. 217, 103934. https://doi.org/10.1016/j. gloplacha.2022.103934.
Lyons, P.C., Millay, M.A., Zodrow, E.L., Cross, A.T., Gillis, K.S., 1995. Discovery of permineralized plant fossils (coal balls) in the Bolsovian (e.g., Westphalian C) (Middle Pennsylvanian, Upper Carboniferous), Stellarton Basin, Nova Scotia, Canada. Can. J. Bot. 73 (9), 1407–1416. https://doi.org/10.1139/b95-153.
Ma, X.X., Li, M.W., Pang, X.Q., Wei, X.Y., Qian, M.H., Tao, G.L., Liu, P., Jiang, Q.G., Li, Z.M., Zhao, Y., 2019. Paradox in bulk and molecular geochemical data and implications for hydrocarbon migration in the inter-salt lacustrine shale oil reservoir, Qianjiang Formation, Jianghan Basin, Central China. Int. J. Coal Geol. 209, 72–88. https://doi.org/10.1016/j.coal.2019.05.005.
Ma, Y.Q., Fan, M.J., Lu, Y.C., Liu, H.M., Hao, Y.Q., Xie, Z.H., Liu, Z.H., Peng, L., Du, X.B., Hu, H.Y., 2016. Climate-driven paleolimnological change controls lacustrine mudstone depositional process and organic matter accumulation: Constraints from lithofacies and geochemical studies in the Zhanhua Depression, eastern China. Int. J. Coal Geol. 167, 103–118. https://doi.org/10.1016/j.coal.2016.09.014.
Mahesh, T.R., Geman, O., Margala, M., Guduri, M., 2023. The stratified K-folds cross-validation and class-balancing methods with high-performance ensemble classifiers for breast cancer classification. Healthcare Anal. 4, 100247. https://doi.org/10.1016/j.health.2023.100247.
Mahynski, N.A., Ragland, J.M., Schuur, S.S., Shen, V.K., 2022. Building interpretable machine learning models to identify chemometric trends in seabirds of the north pacific ocean. Environ. Sci. Technol. 56 (20), 14361–14374. https://doi.org/10.1021/acs.est.2c01894.
Meng, Q.T., Liu, Z.J., Liu, R., Sun, P.C., Hu, F., Zhang, J., 2011. Comparision on the characteristics of biomarkers of oil shale between Huadian Formatin in Huadian Basin and Green River Formation in Uinta Basin of western United States. J Jilin Univ. Sci. Ed. 41 (2), 391–399.
Meng, Q.T., Liu, Z.J., Bruch, A.A., Liu, R., Hu, F., 2012. Palaeoclimatic evolution during Eocene and its influence on oil shale mineralisation, Fushun Basin, China. J. Asian Earth Sci. 45, 95–105. https://doi.org/10.1016/j.jseaes.2011.09.021.
Meyers, S.R., Sageman, B.B., Hinnov, L.A., 2001. Integrated quantitative stratigraphy of the Cenomanian-Turonian Bridge Creek Limestone Member using evolutive harmonic analysis and stratigraphic modeling. J. Sediment. Res. 71 (4), 628–644. https://doi.org/10.1306/012401710628.
Ministry of Land and Resources of China, 2006. National Development and Reform Commission. Ministry of Finance "National Oil Shale Resource Evaluation". Report (In China).
Moldowan, J.M., Seifert, W.K., Gallegos, E.J., 1985. Relationship between petroleum composition and depositional environment of petroleum source rocks. AAPG Bull. 69 (8), 1255–1268. https://doi.org/10.1306/ad462bc8-16f7-11d7-8645000102c1865d.
Moore, S.W., Madrid, H.B., Server, G.T., 1983. Results of Oil-Shale Investigations in Northestern Nevada. U.S. Geological Survey, p. 111.
Moradi, A.V., Sarı, A., Akkaya, P., 2016. Geochemistry of the Miocene oil shale (Hançili Formation) in the Çankırı-Çorum Basin, Central Turkey: implications for paleoclimate conditions, source–area weathering, provenance and tectonic setting. Sediment. Geol. 341, 289–303. https://doi.org/10.1016/j.sedgeo.2016.05.002.
Mukhopadhyay, P.K., Goodarzi, F., Crandlemire, A.L., Gillis, K.S., MacNeil, D.J., Smith, W.D., 1998. Comparison of coal composition and elemental distribution in selected seams of the Sydney and Stellarton Basins, Nova Scotia, Eastern Canada. Int. J. Coal Geol. 37 (1–2), 113–141. https://doi.org/10.1016/S0166-5162(98)00020-2.
Müller, P.J., Suess, E., 1979. Productivity, sedimentation rate, and sedimentary organic matter in the oceans—I. Organic carbon preservation. Deep-Sea Res. Part A 26, 1347–1362. https://doi.org/10.1016/0198-0149(79)90003-7.
Murphy, A.E., Sageman, B.B., Hollander, D.J., Lyons, T.W., Brett, C.E., 2000. Black shale deposition and faunal overturn in the Devonian Appalachian Basin: clastic starvation, seasonal water-column mixing, and efficient biolimiting nutrient recycling. Paleoceanography 15 (3), 280–291. https://doi.org/10.1029/1999PA000445.
Nesbitt, H., Young, G.M., 1982. Early Proterozoic climates and plate motions inferred from major element chemistry of lutites. Nature 299 (5885), 715–717. https://doi.org/10.1038/299715a0.
Nesbitt, H.W., Young, G.M., 1989. Formation and diagenesis of weathering profiles. J. Geol. 97 (2), 129–147. https://doi.org/10.1086/629290.
Ocakoğlu, F., Açıkalın, S., Yılmaz, İ.Ö., Şafak, Ü., Gökçeoğlu, C., 2012. Evidence of orbital forcing in lake-level fluctuations in the Middle Eocene oil shale-bearing lacustrine successions in the Mudurnu-Göynük Basin, NW Anatolia (Turkey). J. Asian Earth Sci. 56, 54–71. https://doi.org/10.1016/j.jseaes.2012.04.021.
O'Dowd, C.D., Facchini, M.C., Cavalli, F., Ceburnis, D., Mircea, M., Decesari, S., Fuzzi, S., Yoon, Y.J., Putaud, J.P., 2004. Biogenically driven organic contribution to marine aerosol. Nature 431 (7009), 676–680. https://doi.org/10.1038/nature02959.
Osterholz, H., Kirchman, D.L., Niggemann, J., Dittmar, T., 2016. Environmental drivers of dissolved organic matter molecular composition in the Delaware Estuary. Earth Sci. Front. 4, 95. https://doi.org/10.3389/feart.2016.00095.
Padula, V.T., 1969. Oil shale of Permian Iratí formation, Brazil. AAPG Bull. 53 (3), 590–602.
Pan, S.F., Pan, N.Q., Tian, H.Q., Friedlingstein, P., Sitch, S., Shi, H., Arora, V.K., Haverd, V., Jain, A.K., Kato, E., 2020. Evaluation of global terrestrial evapotranspiration using state-of-the-art approaches in remote sensing, machine learning and land surface modeling. Hydrol. Earth Syst. Sci. 24 (3), 1485–1509. https://doi.org/10.5194/hess-24-1485-2020.
Patterson, G.W., 1971. The distribution of sterols in algae. Lipids 6 (2), 120–127. https://doi.org/10.1007/bf02531327.
Pedersen, T.F., Calvert, S.E., 1990. Anoxia vs. productivity: what controls the formation of organic-carbon-rich sediments and sedimentary rocks? AAPG Bull. 74 (4), 454–466. https://doi.org/10.1306/0C9B232B-1710-11D7-8645000102C1865D.
Peng, C., Zou, C.C., Pan, L., Niu, Y.X., 2017. Application of geochemical logging for palaeoenvironmental research in the late cretaceous Qingshankou Formation from the Chinese Continental Scientific Drilling Project-SK-2e, Songliao Basin, NE China. J. Geophys. Eng. 14 (4), 865–877. https://doi.org/10.1088/1742-2140/aa6b2f.

Peters, K.E., Walters, C., Moldowan, J.M., 2005. The Biomarker Guide, 2nd edition. Cambridge University Press, Cambridge UK.
Philp, P., Symcox, C., Wood, M., Nguyen, T., Wang, H.D., Kim, D.W., 2021. Possible explanations for the predominance of tricyclic terpanes over pentacyclic terpanes in oils and rock extracts. Org. Geochem. 155, 104220. https://doi.org/10.1016/j.orggeochem.2021.104220.
Philp, R.P., Fan, P., Lewis, C.A., Zhu, H., Wang, H., 1991. Geochemical characteristics of oils from the Chaidamu, Shanganning and Jianghan Basins, China. J. SE Asian Earth Sci. 5 (1–4), 351–358. https://doi.org/10.1016/0743-9547(91)90048-3.
Philp, R.T., Gilbert, T., 1986. Biomarker distributions in Australian oils predominantly derived from terrigenous source material. Org. Geochem. 10 (1–3), 73–84. https://doi.org/10.1016/0146-6380(86)90010-0.
Pietras, J.T., Carroll, A.R., Rhodes, M.K., 2003. Lake basin response to tectonic drainage diversion: Eocene Green River Formation, Wyoming. J. Paleolimnol. 30, 115–125. https://doi.org/10.1023/A:1025518015341.
Powell, T.G., McKirdy, D.M., 1973. Relationship between ratio of pristane to phytane, crude oil composition and geological environment in Australia. Nature 243 (124), 37–39. https://doi.org/10.1038/physci243037a0.
Qiao, J.Q., Baniasad, A., Zieger, L., Zhang, C., Luo, Q., Littke, R., 2021. Paleo-depositional environment, origin and characteristics of organic matter of the Triassic Chang 7 Member of the Yanchang Formation throughout the mid-western part of the Ordos Basin, China. Int. J. Coal Geol. 237, 103636. https://doi.org/10.1016/j.coal.2020.103636.
Qiao, J.Q., Luo, Q.Q., Zhang, Y., Wang, D.D., Cui, H., Shang, X.Q., Liu, L.F., Zhang, T., 2023. Formation conditions and enrichment mechanisms of the Jurassic lacustrine organic-rich shale in the East Fukang Sag, Junggar Basin, NW China: a reassessment based on organic geochemistry. Front. Earth Sci. 11, 1086827. https://doi.org/10.3389/feart.2023.1086827.
Redfield, A.C., 1958. The biological control of chemical factors in the environment. Am. Sci. 46 (3), 230A–221. http://www.jstor.org/stable/27827150.
Reichstein, M., Camps-Valls, G., Stevens, B., Jung, M., Denzler, J., Carvalhais, N., Prabhat, F., 2019. Deep learning and process understanding for data-driven Earth system science. Nature 566 (7743), 195–204. https://doi.org/10.1038/s41586-019-0912-1.
Rimmer, S.M., 2004. Geochemical paleoredox indicators in Devonian–Mississippian black shales, central Appalachian Basin (USA). Chem. Geol. 206 (3–4), 373–391. https://doi.org/10.1016/j.chemgeo.2003.12.029.
Rosenberg, M.J., Birgenheier, L.P., Berg, M.D.V., 2015. Facies, stratigraphic architecture, and lake evolution of the oil shale bearing green river formation, Eastern Uinta Basin, Utah. In: Smith, M.E., Carroll, A.R. (Eds.), Stratigraphy and Paleolimnology of the Green River Formation, Western USA. Springer Nature, Switzerland, pp. 211–249.
Ross, D.J., Bustin, R.M., 2009. Investigating the use of sedimentary geochemical proxies for paleoenvironment interpretation of thermally mature organic-rich strata: Examples from the Devonian–Mississippian shales, Western Canadian Sedimentary Basin. Chem. Geol. 260 (1–2), 1–19. https://doi.org/10.1016/j.chemgeo.2008.10.027.
Sageman, B.B., Murphy, A.E., Werne, J.P., Ver Straeten, C.A., Hollander, D.J., Lyons, T. W., 2003. A tale of shales: the relative roles of production, decomposition, and dilution in the accumulation of organic-rich strata, Middle–Upper Devonian, Appalachian Basin. Chem. Geol. 195 (1–4), 229–273. https://doi.org/10.1016/S0009-2541(02)00397-2.
Samuel, O.J., Kildahl-Andersen, G., Nytoft, H.P., Johansen, J.E., Jones, M., 2010. Novel tricyclic and tetracyclic terpanes in Tertiary deltaic oils: structural identification, origin and application to petroleum correlation. Org. Geochem. 41 (12), 1326–1337. https://doi.org/10.1016/j.orggeochem.2010.10.002.
Sari, A., Aliyev, S.A., 2005. Source rock evaluation of the lacustrine oil shale bearing deposits: Göynük/Bolu, Turkey. Energy Sources 27 (3), 279–298. https://doi.org/10.1080/00908310490441980.
Schenau, S.J., Reichart, G.J., De Lange, G.J., 2005. Phosphorus burial as a function of paleoproductivity and redox conditions in Arabian Sea sediments. Geochim. Cosmochim. Acta 69 (4), 919–931. https://doi.org/10.1016/j.gca.2004.05.044.
Schulte, S., Mangelsdorf, K., Rullkötter, J., 2000. Organic matter preservation on the Pakistan continental margin as revealed by biomarker geochemistry. Org. Geochem. 31 (10), 1005–1022. https://doi.org/10.1016/S0146-6380(00)00108-X.
Schwark, L., Empt, P., 2006. Sterane biomarkers as indicators of Palaeozoic algal evolution and extinction events. Palaeogeogr. Palaeoclimatol. Palaeoecol. 240 (1–2), 225–236. https://doi.org/10.1016/j.palaeo.2006.03.050.
Schwark, L., Vliex, M., Schaeffer, P., 1998. Geochemical characterization of Malm Zeta laminated carbonates from the Franconian Alb, SW-Germany (II). Org. Geochem. 29 (8), 1921–1952. https://doi.org/10.1016/S0146-6380(98)00192-2.
Schwarzkopf, T.A., 1993. Model for prediction of organic carbon content in possible source rocks. Mar. Pet. Geol. 10 (5), 478–492. https://doi.org/10.1016/0264-8172(93)90049-X.
Scotese, C.R., 2016. PALEOMAP PaleoAtlas for GPlates and the PaleoData Plotter Program. PALEOMAP Project. *http*://www.earthbyte.org/paleomap-paleoatlas-for-gplates.
Scotese, C.R., Song, H., Mills, B.J., van der Meer, D.G., 2021. Phanerozoic paleotemperatures: the earth's changing climate during the last 540 million years. Earth Sci. Rev. 215, 103503. https://doi.org/10.1016/j.earscirev.2021.103503.
Şener, M., Şengüler, İ., 1992. Geology, Usage Facility and Firing Test Results in Fluid Bed of Seyitömer Oil Shale. Report No. 9441, MTA, Ankara. http://www.mta.gov.tr/v3.0/hizmetler/derleme-ara.
Şener, M., Şengüler, I., Kök, M.V., 1995. Geological considerations for the economic evaluation of oil shale deposits in Turkey. Fuel 74 (7), 999–1003. https://doi.org/10.1016/0016-2361(95)00045-7.
Şener, M., Şengüler, I., Taka, M., Şener, M.F., 2013. The stratigraphic, mineralogical, and geochemical characterization of the Beypazarı oil shales, Central Anatolia, Turkey. Energy Sourc. Part A 35 (18), 1741–1752. https://doi.org/10.1080/15567036.2010.531502.
Sheldon, N.D., Tabor, N.J., 2009. Quantitative paleoenvironmental and paleoclimatic reconstruction using paleosols. Earth Sci. Rev. 95 (1–2), 1–52. https://doi.org/10.1016/j.earscirev.2009.03.004.
Shi, J.H., Guan, Y., Gao, H.W., Yao, X.H., Wang, R.Z., Zhang, D.Z., 2022. Aerosol iron solubility specification in the global marine atmosphere with machine learning. Environ. Sci. Technol. 56 (22), 16453–16461. https://doi.org/10.1021/acs.est.2c05266.
Shi, J.Y., Jin, Z.J., Liu, Q.Y., Huang, Z.K., Hao, Y.Q., 2018. Terrestrial sedimentary responses to astronomically forced climate changes during the early Paleogene in the Bohai Bay Basin, eastern China. Palaeogeogr. Palaeoclimatol. Palaeoecol. 502, 1–12. https://doi.org/10.1016/j.palaeo.2018.01.006.
Singh, A., Thakur, N., Sharma, A., 2016. A review of supervised machine learning algorithms. In: 2016 3rd International Conference on Computing for Sustainable Global Development (INDIACom), New Delhi, India, pp. 1310–1315.
Sinninghe Damsté, J.S., Kenig, F., Koopmans, M.P., Köster, J., Schouten, S., Hayes, J., de Leeuw, J.W., 1995. Evidence for gammacerane as an indicator of water column stratification. Geochim. Cosmochim. Acta 59 (9), 1895–1900. https://doi.org/10.1016/0016-7037(95)00073-9.
Skomurski, F.N., Ilton, E.S., Engelhard, M.H., Arey, B.W., Rosso, K.M., 2011. Heterogeneous reduction of $U^{6}+$ by structural Fe^{2+} from theory and experiment. Geochim. Cosmochim. Acta 75 (22), 7277–7290. https://doi.org/10.1016/j.gca.2011.08.006.
Smith, M.E., Singer, B., Carroll, A., 2003. $^{40}Ar/^{39}Ar$ geochronology of the Eocene Green River Formation, Wyoming. Geol. Soc. Am. Bull. 115 (5), 549–565. https://doi.org/10.1130/0016-7606(2003)115<0549:agoteg>2.0.co;2.
Smith, W.D., Peter, C.S., Naylor, R.D., Mukhopadhyay, P.K., Kalkreuth, W.D., Ball, F.D., Macauley, G., 1991. Composition and depositional environment of major eastern Canadian oil shales. Int. J. Coal Geol. 19 (1–4), 385–438. https://doi.org/10.1016/0166-5162(91)90028-H.
Stevens, S.H., Moodhe, K.D., Kuuskraa, V.A., 2013. China Shale Gas and Shale Oil Resource Evaluation and Technical Challenges, SPE Asia Pacific Oil and Gas Conference and Exhibition. SPE, pp. SPE-165832-MS.
Strobl, S.A., Sachsenhofer, R.F., Bechtel, A., Gratzer, R., Gross, D., Bokhari, S.N., Liu, R., Liu, Z.J., Meng, Q.T., Sun, P.C., 2014. Depositional environment of oil shale within the Eocene Jijuntun Formation in the Fushun Basin (NE China). Mar. Pet. Geol. 56, 166–183. https://doi.org/10.1016/j.marpetgeo.2014.04.011.
Sun, F.N., Hu, W.X., Cao, J., Wang, X.L., Zhang, Z.R., Ramezani, J., Shen, S.Z., 2022. Sustained and intensified lacustrine methane cycling during early Permian climate warming. Nat. Commun. 13 (1), 4856. https://doi.org/10.1038/s41467-022-32438-2.
Surdam, R.C., Stanley, K., 1979. Lacustrine sedimentation during the culminating phase of Eocene lake Gosiute, Wyoming (Green River Formation). Geol. Soc. Am. Bull. 90 (1), 93–110. https://doi.org/10.1130/0016-7606(1979)90<93:LSDTCP>2.0.CO;2.
Suwannathong, A., Khummongkol, D., 2007. Oil Shale Resources in Mae Sot Basin, Thailand. Oil Shale 15, 17.
Sweere, T., van den Boorn, S., Dickson, A.J., Reichart, G.J., 2016. Definition of new trace-metal proxies for the controls on organic matter enrichment in marine sediments based on Mn, Co, Mo and Cd concentrations. Chem. Geol. 441, 235–245. https://doi.org/10.1016/j.chemgeo.2016.08.028.
Taka, M., Şener, M., 1988. Oil Shale Facility of Himmetoğlu (Göynük-Bolu) Field and their Wells. No. 8533, MTA, Ankara, Report.
Tappan, H.N., 1980. The Palaeobiology of Plant Protists. Freeman, San Francisco, p. 1028.
Taylor, S.R., McLennan, S.H., 1985. The Continental Crust: Its Composition and Evolution. Blackwell, Oxford, p. 312.
Ten Haven, H.L., De Leeuw, J.W., Rullkötter, J., Sinninghe Damsté, J.S., 1987. Restricted utility of the pristane/phytane ratio as a palaeoenvironmental indicator. Nature 330 (6149), 641–643. https://doi.org/10.1038/330641a0.
Tissot, B.P., Welte, D.H., 1984. Petroleum Formation and Occurrence–Second Revised and, enlarged edition. Springer-Verlag, Berlin Heidelberg, NY, pp. 160–198.
Trewartha, G.T., Horn, L.H., 1980. An Introduction to Climate, 5th ed. McGraw-Hill, NY, p. 416.
Tribovillard, N., Algeo, T.J., Lyons, T., Riboulleau, A., 2006. Trace metals as paleoredox and paleoproductivity proxies: an update. Chem. Geol. 232 (1–2), 12–32. https://doi.org/10.1016/j.chemgeo.2006.02.012.
Tribovillard, N., Algeo, T.J., Baudin, F., Riboulleau, A., 2012. Analysis of marine environmental conditions based on molybdenum–uranium covariation—applications to Mesozoic paleoceanography. Chem. Geol. 324, 46–58. https://doi.org/10.1016/j.chemgeo.2011.09.009.
Tulipani, S., Grice, K., Greenwood, P.F., Schwark, L., Böttcher, M.E., Summons, R.E., Foster, C.B., 2015. Molecular proxies as indicators of freshwater incursion-driven salinity stratification. Chem. Geol. 409, 61–68. https://doi.org/10.1016/j.chemgeo.2015.05.009.
Tyson, R.V., 1995. Abundance of organic matter in sediments: TOC, hydrodynamic equivalence, dilution and flux effects. In: Sedimentary Organic Matter. Springer, Dordrecht, pp. 81–118. https://doi.org/10.1007/978-94-011-0739-6_5.
Tyson, R.V., 2001. Sedimentation rate, dilution, preservation, and total organic carbon: some results of a modeling study. Org. Geochem. 32, 333–339. https://doi.org/10.1016/S0146-6380(00)00161-3.
Walker, W.J., Cronan, C.S., Patterson, H.H., 1988. A kinetic study of aluminum adsorption by aluminosilicate clay minerals. Geochim. Cosmochim. Acta 52 (1), 55–62. https://doi.org/10.1016/0016-7037(88)90056-7.

Walters, A.P., Meyers, S.R., Carroll, A.R., Hill, T.R., Vanden Berg, M.D., 2020. Lacustrine cyclicity in the early Eocene Green River Formation, Uinta Basin, Utah: evidence from X-ray fluorescence core scanning. J. Sediment. Res. 90 (4), 429–447. https://doi.org/10.2110/jsr.2020.24.

Wang, A.G., Li, C.Y., Li, L., Pu, R.H., Yang, Z.G., Zhu, N., Guo, K., 2023a. C_{20}-C_{21}-C_{23} tricyclic terpanes abundance patterns: Origin and application to depositional environment identification. Front. Earth Sci. 11, 1128692. https://doi.org/10.3389/feart.2023.1128692.

Wang, L., Song, Z.G., Yin, Q., George, S.C., 2011. Paleosalinity significance of occurrence and distribution of methyltrimethyltridecyl chromans in the Upper cretaceous Nenjiang Formation, Songliao Basin, China. Org. Geochem. 42 (11), 1411–1419. https://doi.org/10.1016/j.orggeochem.2011.08.012.

Wang, L., Liu, B., Bai, L.H., Ostadhassan, M., Gentzis, T., Wang, B.Y., Wang, Y.Z., 2023b. Maceral evolution of lacustrine shale and its effects on the development of organic pores during low mature to high mature stage: a case study from the Qingshankou Formation in northern Songliao Basin, Northeast China. Pet. Sci. 20 (5), 2709–2725. https://doi.org/10.1016/j.petsci.2023.08.025.

Wang, P., Du, Y.S., Yu, W.C., Algeo, T.J., Zhou, Q., Xu, Y., Qi, L., Yuan, L.J., Pan, W., 2020. The chemical index of alteration (CIA) as a proxy for climate change during glacial-interglacial transitions in Earth history. Earth Sci. Rev. 201, 103032. https://doi.org/10.1016/j.earscirev.2019.103032.

Wang, T.T., Cao, J., Xia, L.W., Zhi, D.M., Tang, Y., He, W.J., 2022. Revised age of the Fengcheng Formation, Junggar Basin, China: Global implications for the late Paleozoic Ice Age. Glob. Planet. Chang. 208, 103725. https://doi.org/10.1016/j.gloplacha.2021.103725.

Wang, X.L., Algeo, T.J., Li, C., Zhu, M.Y., 2023c. Spatial pattern of marine oxygenation set by tectonic and ecological drivers over the Phanerozoic. Nat. Geosci. 16 (11), 1020–1026. https://doi.org/10.1038/s41561-023-01296-y.

Wang, Z.W., Fu, X.G., Feng, X.L., Song, C.Y., Wang, D., Chen, W.B., Zeng, S.Q., 2017. Geochemical features of the black shales from the Wuyu Basin, southern Tibet: implications for palaeoenvironment and palaeoclimate. Geol. J. 52 (2), 282–297. https://doi.org/10.1002/gj.2756.

Warren, J.K., 2010. Evaporites through time: Tectonic, climatic and eustatic controls in marine and nonmarine deposits. Earth Sci. Rev. 98 (3–4), 217–268. https://doi.org/10.1016/j.earscirev.2009.11.004.

Warren, J.K., 2016. Evaporites: A geological compendium. Springer, Berlin, pp. 1–1079.

Wicaksono, P., Lazuardi, W., 2018. Assessment of PlanetScope images for benthic habitat and seagrass species mapping in a complex optically shallow water environment. Int. J. Remote Sens. 39 (17), 5739–5765. https://doi.org/10.1080/01431161.2018.1506951.

Woodhouse, A.D., Oung, J.N., Philp, R.P., Weston, R.J., 1992. Triterpanes and ring-a degraded triterpanes as biomarkers characteristic of Tertiary oils derived from predominantly higher plant sources. Org. Geochem. 18 (1), 23–31. https://doi.org/10.1016/0146-6380(92)90140-S.

Wright, J.A., Hoffe, B.H., Langdon, G.S., Quinlan, G.M., 1996. The deer Lake Basin, Newfoundland: structural constraints from new seismic data. Bull. Can. Petrol. Geol. 44 (4), 674–682. https://doi.org/10.35767/gscpgbull.44.4.674.

Wu, P., Hou, D.J., Cao, L.Z., Zheng, R.H., Wei, X.L., Ma, X.X., Zhao, Z., Chen, J.W., 2023. Paleoenvironment and organic characterization of the lower cretaceous lacustrine source rocks in the Erlian Basin: the influence of hydrothermal and volcanic activity on the source rock quality. ACS Omega 8 (2), 1885–1911. https://doi.org/10.1021/acsomega.2c03487.

Xu, C., Hu, F., Meng, Q.T., Liu, Z.J., Shan, X.L., Zeng, W.R., Zhang, K., He, W.T., 2022. Organic matter accumulation in the Youganwo Formation (Middle Eocene), Maoming Basin, South China: Constraints from multiple geochemical proxies and organic petrology. ACS Earth Space Chem. 6 (3), 714–732. https://doi.org/10.1021/acsearthspacechem.1c00383.

Xu, L.X., 1995. Chronology of Paleogene volcanic rocks in the Jianghan Basin. Oil Gas Geol. 16, 132–137.

Xu, S., Wang, Y.X., Bai, N., Wu, S.Q., Liu, B.C., 2024. Organic matter enrichment mechanism in saline lacustrine basins: a review. Geol. J. 59 (1), 155–168. https://doi.org/10.1002/gj.4853.

Xu, S.C., Liu, Z.J., Zhang, P., Boak, J.M., Liu, R., Meng, Q.T., 2016. Characterization of depositional conditions for lacustrine oil shales in the Eocene Jijuntun Formation, Fushun Basin, NE China. Int. J. Coal Geol. 167, 10–30. https://doi.org/10.1016/j.coal.2016.09.004.

Xu, W.M., Ruhl, M., Jenkyns, H.C., Leng, M.J., Huggett, J.M., Minisini, D., Ullmann, C.V., Riding, J.B., Weijers, J.W., Storm, M.S., 2018. Evolution of the Toarcian (early Jurassic) carbon-cycle and global climatic controls on local sedimentary processes (Cardigan Bay Basin, UK). Earth Planet. Sci. Lett. 484, 396–411. https://doi.org/10.1016/j.epsl.2017.12.037.

Yang, H., Zhang, W.Z., 2005. Leading effect of the Seventh Member high-quality source rock of Yanchang Formation in Ordos Basin during the enrichment of low-penetrating oil-gas accumulation: Geology and geochemistry. Geochimica 34 (2), 147–154.

Yanilmaz, E., Ipeksever, M., Aslan, N., 1980. Report on Gölpazarı (Bilecik) Oil Shale Field, Report No. 7060, MTA, Ankara.

Yawanarajah, S.R., Kruge, M.A., 1994. Lacustrine shales and oil shales from Stellarton Basin, Nova Scotia, Canada: organofacies variations and use of polyaromatic hydrocarbons as maturity indicators. Org. Geochem. 21 (2), 153–170. https://doi.org/10.1016/0146-6380(94)90152-X.

Yin, J., Xu, C.G., Hao, F., Wang, Q., Miao, Q.Y., Wang, Z.Q., Zou, H.Y., 2020. Controls on organic matter enrichment in source rocks of the Shahejie Formation in the southwestern Bozhong Sag, Bohai Bay Basin, China. Palaeogeogr. Palaeoclimatol. Palaeoecol. 560, 110026. https://doi.org/10.1016/j.palaeo.2020.110026.

Young, G.M., Nesbitt, H.W., 1998. Processes controlling the distribution of Ti and Al in weathering profiles, siliciclastic sediments and sedimentary rocks. J. Sediment. Res. 68 (3), 448–455. https://doi.org/10.2110/jsr.68.448.

Yu, K.H., Cao, Y.C., Qiu, L.W., Sun, P.P., 2019. Depositional environments in an arid, closed basin and their implications for oil and gas exploration: the lower Permian Fengcheng Formation in the Junggar Basin, China. AAPG Bull. 103 (9), 2073–2115. https://doi.org/10.1306/01301917414.

Zhang, K., Liu, R., Liu, Z.J., Li, B., Han, J.B., Zhao, K.G., 2020. Influence of volcanic and hydrothermal activity on organic matter enrichment in the Upper Triassic Yanchang Formation, southern Ordos Basin, Central China. Mar. Pet. Geol. 112, 104059. https://doi.org/10.1016/j.marpetgeo.2019.104059.

Zhang, K., Liu, R., Liu, Z.J., 2021a. Sedimentary sequence evolution and organic matter accumulation characteristics of the Chang 8–Chang 7 members in the Upper Triassic Yanchang Formation, Southwest Ordos Basin, Central China. J. Pet. Sci. Eng. 196, 107751. https://doi.org/10.1016/j.petrol.2020.107751.

Zhang, K., Liu, R., Liu, Z.J., Li, L., 2021b. Geochemical characteristics and geological significance of humid climate events in the Middle-late Triassic (Ladinian-Carnian) of the Ordos Basin, Central China. Mar. Pet. Geol. 131, 105179. https://doi.org/10.1016/j.marpetgeo.2021.105179.

Zhang, M.Z., Dai, S., Pan, S.Q., Jing, Z.H., Wu, Z.X., Chen, Y.X., Du, B.X., Zhang, J., Liu, G.L., Jiaoba, D.Z., 2023. Deciphering the laminated botryococcus-dominated shales in saline lacustrine basin, Western Qaidam Basin, NW China: Implications for shale oil potential. Mar. Pet. Geol. 155, 106397. https://doi.org/10.1016/j.marpetgeo.2023.106397.

Zhang, Y.Q., Dong, S.W., Li, J.H., Shi, W., 2011. Mesozoic multi-directional compressional tectonics and formation-reformation of Sichuan Basin (in Chinese with English abstract). Geol. China 38 (2), 233–250.

Zhao, R., Chen, S., Wang, H., Yan, D.T., Cao, H.Y., Gong, Y., He, J., Wu, Z.X., 2019. Paleogene sedimentation changes in Lenghu Area, Qaidam Basin in response to the India–Eurasia collision. Int. J. Earth Sci. 108, 27–48. https://doi.org/10.1007/s00531-018-1640-8.

Zheng, D.R., Nel, A., Wang, H., Wang, B., Jarzembowski, E.A., Chang, S.C., Zhang, H.C., 2017. The first late Triassic Chinese triadophlebiomorphan (Insecta: Odonatoptera): biogeographic implications. Sci. Rep. 7 (1), 1476. https://doi.org/10.1038/s41598-017-01710-7.

Zheng, Y.W., Fu, D.L., Tian, B., Duan, Z.Q., Zhang, B., Luo, J.N., Wang, Z.X., 2021. The mineral composition and geochemical characteristics of rare earth elements of salt lake shale in Qianjiang Depression and its geological significance (in Chinese with English abstract). Marine Origin Petrol. Geol. 26 (02), 150–158. https://link.cnki.net/urlid/33.1328.P.20210611.1021.002.

Zhou, J.T., Yu, W.C., Wei, W., Yang, M.Y., Du, Y.S., 2023. Provenance and tectonic evolution of bauxite deposits in the Tethys: Perspective from random forest and logistic regression analyses. Geochem. Geophys. Geosyst. 24 (6), e2022GC010745. https://doi.org/10.1029/2022GC010745.

Zhu, C.F., Cui, X.Q., He, Y.X., Kong, L.S., Sun, Y.G., 2020a. Extended 3β-methylhopanes up to C_{45} in source rocks from the Upper cretaceous Qingshankou Formation, Songliao Basin, Northeast China. Org. Geochem. 142, 103998. https://doi.org/10.1016/j.orggeochem.2020.103998.

Zhu, F., Li, C.X., Leng, J.Y., Jia, M.Y., Gong, H.J., Wang, B., Zhang, F., Jiang, Z.X., Wang, Z.P., 2023. Paleoenvironmental characteristics of lacustrine shale and its impact on organic matter enrichment in Funing Formation of Subei Basin. Minerals 13 (11), 1439. https://doi.org/10.3390/min13111439.

Zhu, R.K., Cui, J.W., Luo, Z., Li, S., Mao, Z.G., Xi, K.L., Su, L., 2020b. Isotopic geochemical characteristics of two types of carbonate concretions of Chang 7 member in the Middle-Upper Triassic Yanchang Formation, Ordos Basin, Central China. Mar. Pet. Geol. 116, 104312. https://doi.org/10.1016/j.marpetgeo.2020.104312.

Zimmerle, W., 1985. New aspects on the formation of hydrocarbon source rocks. Geol. Rundsch. 74 (2), 385–416. https://doi.org/10.1007/BF01824905.

Zirks, E., Krom, M., Schmiedl, G., Katz, T., Xiong, Y., Alcott, L.J., Poulton, S.W., Goodman-Tchernov, B., 2021. Redox evolution and the development of oxygen minimum zones in the Eastern Mediterranean Levantine Basin during the early Holocene. Geochim. Cosmochim. Acta 297, 82–100. https://doi.org/10.1016/j.gca.2021.01.009.

Zou, C.N., Zhu, R.K., Chen, Z.Q., Ogg, J.G., Wu, S.T., Dong, D.Z., Qiu, Z., Wang, Y.M., Wang, L., Lin, S.H., 2019. Organic-matter-rich shales of China. Earth-Sci. Rev. 189, 51–78. https://doi.org/10.1016/j.earscirev.2018.12.002.